Spring 2013

Effects of material variables and process parameters on properties of investment casting shells

Priyatham Tumurugoti

Department:

EFFECTS OF MATERIAL VARIABLES AND PROCESS PARAMETERS ON PROPERTIES OF INVESTMENT CASTING SHELLS

by

PRIYATHAM TUMURUGOTI

A THESIS

Presented to the Faculty of the Graduate School of the

MISSOURI UNIVERSITY OF SCIENCE AND TECHNOLOGY

In Partial Fulfillment of the Requirements for the Degree

MASTER OF SCIENCE IN MATERIALS SCIENCE AND ENGINEERING

2013

Approved by

Jeffrey D. Smith, Advisor

Von L. Richards

Simon N. Lekakh

ABSTRACT

Manufacture of investment casting shells is a complex process. The choice of raw materials - refractory powders or grains, binders and additives - affects the properties of investment casting shells. In this study, different systems of shells were prepared, according to a design of experiments, with commercially available raw materials that differ in chemistry, particle size or particle size distribution. Shell strength was measured in green, fired and cooled, and hot conditions and the results were analyzed for strength – material property relation. Various microstructures of polished cross sections of these shells were characterized using scanning electron microscope. It was determined that the amount of matrix holding the stucco grains was dominant factor affecting green strength. Fired and hot strengths were observed to vary depending on interactions between different phases of matrix and stucco.

In addition to the material properties, control of shell building parameters is critical to achieve quality shells. Process parameters affect strength of the shell by providing a means to change the relative amounts of stucco, slurry and porosity. To study the microstructural variations, shells were prepared by varying process parameters like slurry viscosity and stucco size. Data from image analysis of different microstructures were correlated to their respective fired strengths. It was determined that the shells prepared from high viscosity slurry and fine stucco had the highest strength.

ACKNOWLEDGMENTS

I would like to thank Dr. Jeffrey Smith and Dr. Von Richards for their valuable assistance throughout this research. Their valuable guidance and feedback had been of great help. I would also thank the U.S. Army Benet Laboratories for funding this research.

I also express my gratitude to Dr. Simon Lekakh for guiding me with the research plan and experiments. I would like to acknowledge the help of fellow members of the research group, Mingzhi Xu and Samrat Bharadwaj, in making samples and conducting experiments. Also, the assistance by other graduate and undergraduate students is appreciated. I would also like to thank the foundries that supported this research with their technical inputs.

I am very grateful to my parents and brothers who have been a constant support and encouragement for my education.

TABLE OF CONTENTS

Page

LIST OF ILLUSTRATIONS

LIST OF TABLES

1. INTRODUCTION

Investment casting, one of the oldest casting processes, is used to fabricate near-net-shaped products. The basic technique of investment casting process has been known and used for centuries in the form of "lost-wax" process.[1] Demand for finished, precision parts for arms and aircraft, during World War II, laid foundations for the modern investment casting industry.[2] Growth has continued until the present with an increased number of applications in commercial market.

Investment casting involves using an expendable pattern, in the shape of the desired product, made from wax or a material that can be melted away easily. The term investment casting derives from the characteristic use of mobile ceramic slurries, or 'investments' to form molds with an extremely smooth surface.[1] The pattern is then melted out from the mold by heating, leaving a hard ceramic mold. The liquid metal is then poured to form the casting.

1.1. PROCESS OVERVIEW

1.1.1. Pattern Making. The investment casting process begins with pattern making; each casting requiring a unique pattern. Patterns are made by injecting the pattern material, generally waxes, into metallic molds of required shape.[3] Tooling and equipment for wax injection depends on the shape of the product. Costlier and sophisticated equipment that can operate at high pressures have to be used for complex shaped patterns demanding high precision. Cost and time savings can be obtained through the use of additive fabrication technology, FDM (Fused Deposition Modeling). FDM is a rapid prototyping technique that uses an STL file (standardized computer file

that contains 3D model) as input. Patterns can also be machined directly from the material, if smaller numbers are required.

The patterns, depending on the size, can be processed individually or can be clustered together to form a single large pattern tree. The gating components and pouring cup are prepared separately and are attached to the pattern forming a pattern assembly. (Figure 1.1)

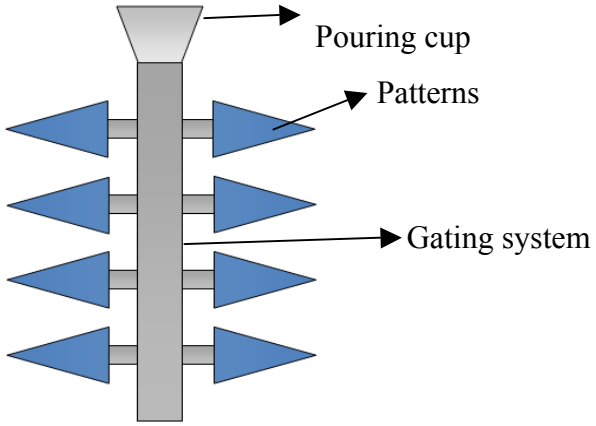

Figure 1.1. Pattern assembly showing cluster of patterns connected together to a gating system

1.1.2. Shell Construction. A multilayer ceramic shell is constructed around the pattern assembly. The first step in the process involves dipping the pattern into a slurry that contains fine refractory powder (flour) and a binder. Then it is taken out and the excess slurry is allowed to drain out to achieve a uniform coating. The first coating provides a smooth surface finish for the casting. This is called ‘primary coat’. Coarse refractory particles (stucco) are then sprinkled onto the slurry layer, embedding the particles on to the outer surface. This process is referred to as stuccoing. These layers are alternatively applied to provide the desired shell thickness. The final stucco layer is often

covered by slurry to encapsulate the final stucco particles. This final coating is called ‘seal coat’. Shells are then dried in air, allowing the binder to polymerize forming a hard gel that holds the stucco particles in the mold.

1.1.3. Pattern Removal. Autoclave dewaxing is the common method for pattern removal.[3] It involves heating the pattern and shell in a pressurized chamber with saturated steam. Pattern and shell get heated from outside and the surface layer of the pattern melts first before the temperature of the inner material increases. This prevents stress effects on the shell that might result from expansion of the pattern material. Flash dewaxing is another process, generally used for plastic patterns, where the pattern is placed in a hot furnace preheated to a high temperature around 1000°C. This introduces large heat flux which melts all pattern material quickly minimizing stress effects.

The ceramic shell molds are then fired in a furnace to completely remove moisture from the shells and also to remove any pattern material left in the shells.

1.1.4. Casting. The fired shells are inspected for cracks and repaired as necessary, using slurry or cement. Then they are washed to remove any residual pattern material. Before pouring the hot metal into the molds, they are preheated (preheating temperature depending up on the metal being cast) to minimize the impact of the sudden temperature rise during the pouring process and to aid the liquid metal to fill in thin sections. Once the pouring is complete, the casting is allowed to cool and the shell is removed. This step of the process can be time consuming and efficient removal of the shell depends on many factors including shell properties (strength, erosion resistance, hardness etc), type of technique used to knock off the shell, temperature etc.[4]

2. LITERATURE REVIEW

2.1.CERAMIC SHELL MOLDS AND REQUIREMENTS

Investment casting shell molds consist of alternate layers of stucco and slurry. Slurry is a mixture of fine refractory filler particles called 'flour' and a colloidal binder system that, upon polymerization, holds these flour particles together. It is typical to use very fine (-325 mesh) filler material for slurry used in primary coat and coarser particles (-200 mesh) for back-up coats. Stuccoing facilitates mechanical bonding between primary and backup coats. These stucco particles also increase the number of stress concentration centers, which reduce the local drying stresses.[1]

Investment casting shells undergo a variety of mechanical and thermal conditions at different stages of the casting process and hence, have different requirements. Failure of the shells is often due to inadequate strength. The main focus of this research is to evaluate different parameters that affect shell strength. Analysis of shell strength in green, fired and hot conditions is necessary to evaluate the integrity of the shell throughout the process.

2.1.1. Green Strength. It is strength of the shell at room temperature that is measured after drying and before firing. It is required for the shell to handle the mechanical stresses during shell building process. Stresses develop within the shell during dip coating and drying, compressive or tensile stresses due to pattern expansion when temperature changes during drying. More importantly, green strength is required to resist the stresses that develop during dewaxing or pattern removal.

2.1.2. Fired Strength. Before pouring the liquid metal and after dewaxing or pattern removal, the shells are fired and cooled so that strength is imparted. At a minimum, the shell should have enough strength during pouring to withstand the weight of hot metal.

2.1.3. Hot Strength. The shells are pre-heated to a high temperature before pouring to minimize thermal shock when the liquid metal is poured. Preheat temperature depends on the metal being cast, normally ranging from 600°C to 1200°C. Depending on the alloy that is being cast, shell should be strong enough not to crack and should have high deformation resistance to produce accurate casting dimensions.

2.1.4. Permeability. Permeability of the shells, both in green and hot conditions, is another important property that determines the quality of the casting. The green shells have to be sufficiently permeable to remove the gases evolved or the wax liquids during the pattern removal. Hot permeability is the measure of permeability of the shells at casting temperatures. Permeability should be high enough to ensure the removal of entrapped air in the molds while pouring so that there is no 'misrun' of the casting. Misrun occurs when the liquid metal does not fill the mold cavity completely due to the back pressure of the entrapped gases.

A summary of required properties of the shells at different stages of the casting process is presented in Table 2.1. The range values mentioned for these properties are based on industrial shells' properties and literature. The desired requirements can be achieved by careful selection of materials and control of the process parameters. The properties of the shells can be altered at different stages depending on:

(a) Material selection: Chemistry, particle size, particle size distribution of flour, stucco and binder

(b) Process parameters: Slurry parameters (flour/binder ratio, viscosity etc), dipping time, drying time, stuccoing parameters (stuccoing time, type of stuccoing), thermal processing (pattern removal, firing, pouring)

Table 2.1. Key requirements for investment casting shells during the entire process

Stage	Key requirements for the shell molds
Slurry coating, drying	High green strength to withstand drying stresses (2 - 4 MPa)
Dewaxing or pattern removal	High green strength (4 - 8 MPa) to resist the forces exerted by the expanding pattern at high temperatures
	Enough permeability to let in condensed steam in autoclave and let out liquid wax or any gases from the decomposing pattern
Pouring	High fired strength to hold the pressures while pouring metal (7 - 10 MPa)
	Deformation resistance at high temperatures to achieve dimensional accuracy (strain < 0.2 %)
	Thermal conductivity as required (0.5 - 3 W/m.K)
	Sufficient permeability to remove entrapped air in the mold (2 - 5 mDarcy)
	Thermal shock resistant for the stability of the mold
Shell knock out	Low strength (4 – 5 MPa)

2.2. MANUFACTURE OF CERAMIC SHELL MOLDS

The manufacture of ceramic shell molds is a complex process involving dipping the pattern in the slurry, stuccoing and drying. The total time for preparation of a mold can extend up to 2-3 days. Each stage of the process should be carefully controlled and monitored for an efficient shell build.

2.2.1. Slurry Preparation and Control. Slurry preparation and control is an important operation in the investment casting process. Viscosity, pH, binder/filler ratio etc., are the parameters that are to be controlled. The generally practiced method for making slurries is:

a) Weigh the binder and filler individually.

b) Pour the binder into a mixing tank and start the mixer.

c) Add the filler in small quantities to the tank, with the mixer running to make sure that there are no lumps.

d) Adjust to the required viscosity by addition of distilled water.

Newly built slurries are allowed to stabilize. Slurry is considered 'stable' if no change in viscosity is observed when measured at one-hour intervals.[5] Slurries for primary coat and back-up coats are prepared separately since they have different requirements. The primary coat slurries tend to have higher viscosities (800 - 1000 cP) and lower viscosities (400-600 cP) are used for back-up coat slurries.

Boccalini Jr. and Correa[6] investigated the effects of binder/filler ratio on strength and permeability of the ceramic shell molds at high temperature (1050°C). Binder/filler ratio was expressed as R_A, which was defined as the ratio between the total surface area of solids in the binder to the total area of filler particles (flour). On increasing R_A, the

strength increased, reached a maximum and then decreased. Increase in R resulted in number of contact points between refractory particles and binder solids. Hence during drying and sintering microcracks form and the observed strength and permeability were high. Very high R_A resulted in excess of solid gel network between refractory particles and this facilitated for the formation of continuous microcracks which reduced the strength and increased the permeability.

Viscosity is an important parameter that characterizes slurry. Measuring viscosity at regular intervals is the most widely employed slurry control technique in foundries. Rusher[7] observed that at a given R_A, viscosity had little effect on shell strength. Similar results were seen from Charles H. Matzek's work[8]. D.M. Kline[9] observed that shell strength remained unchanged with at higher viscosities (>500 cP), but at lower viscosities, a specific trend was not followed. An increase in slurry viscosity resulted in thicker shells and the load bearing capacity increased. Studying the results from above literature, if the layered structure is retained by changing the viscosity, strength did not change. At lower viscosities, where there would be lot of draining of slurry, the cross section of the shell will no longer be a layered one and hence strength changes. The permeability of primary coat of the shell is a dominant factor that determines the overall permeability of the shell.[9]

The pH of the binder also affects the slurry quality and life. Lowering the pH of the colloidal silica binder reduces the repulsive forces between the SiO_2 particles. As a result, the particles may collide and gelling may occur.[7] To control this effect, colloidal silica binder is commonly stabilized at alkaline pH.

2.2.2. Stuccoing. It is usual to select very fine grade of stucco (-50+100 mesh) for primary coat stuccoing to avoid 'stucco penetration'. Stucco penetration refers to a condition in which the stucco, as it strikes the wet slurry, penetrates to the metal face of the mold drawing air pockets and producing small voids in the primary coat, which metal may then penetrate at the time of casting.[1] Hence high viscosity slurry (800 - 1000 cP) is used for primary coat.

Fluidized bed and rainfall sander are two common methods employed industrially for stuccoing. In fluidized bed method, the stucco particles are suspended and move freely, like a fluid, inside a chamber by the injection of compressed air from below. These particles get deposited on the pattern which is held in the chamber. A narrow particle size distribution is important for fluidized bed techniques since there might be segregation of light particles at the top and heavier particles at the bottom of the chamber. Particle size distribution is regarded as narrow when all the material exists between three screens in a standard sieve analysis.[10] Wide particle size distribution might result in inconsistent shell thickness, permeability and strength properties.[10]

The rainfall sander is becoming increasingly popular. Stucco is constantly sprinkled onto the pattern from a fixed height by means of a rotating paddle wheel. Vibrating mesh arrangement can be used in the sander to control the particle size range. The particles that do not adhere to the pattern are reused in the process.

Jones et al. studied the structural and mechanical properties of shells made from both fluidized bed and rainfall sander methods.[11] They found that the fracture strength of shells made using the rainfall process was higher, when all other parameters were equal. Stucco deposited from a height had kinetic energy which helped to embed particles into

the slurry layer. In fluidized bed processing, the stucco particles are swept across the slurry layer and the stucco does not typically penetrate into the slurry. This leaves some amount of slurry untouched and fracture can occur through the slurry matrix without any crack deflection provided by the stucco.

The type and size of stucco material are important factors that affect the properties of shells. The generally used materials for stucco are discussed in subsequent sections. Charles H. Maztek[8] studied the effects of viscosity and stucco size on shell properties. Increase in stucco size increased thickness of the shells for the same number of layers and so the load bearing capacity increased. Minor variation in the fired strength, 7.2 MPa to 8.6 MPa, was observed when stucco size was changed from -16+30 mesh to -20+50 mesh.

2.2.3. Drying. Drying of the coatings in a shell system is normally under constant conditions of humidity, airflow and temperature to ensure similar properties for all molds. Hardening of the coatings occurs during the drying process as the water is evaporated.

Manuel Guerra Jr.'s[12] experiments proved that the maximum green and fired strengths (MOR) were obtained for drying time of four hours between dips. It was observed that the variation in strength was negligible on increasing final drying time, after seal coat, to 12 and 24 hours. But high drying times always reduced the risk of cracking during autoclave firing. Any residual moisture during firing can be detrimental to the shell because of the large expansion that occurs when water converts into steam.

2.2.4. Seal Coat. A seal coat is applied as the final coating to the mold by dipping the mold into slurry and allowing to dry. This is done generally to seal the loose stucco particles from falling from the mold during further processing like firing and

pouring. It also produces a relatively smooth surface that would ease the handling of the mold. Another common practice in many foundries is to apply a second seal coat after the dewaxing operation. This is done whether or not there is a visible crack after dewaxing. However, the seal coat has a significant impact on the properties of the shell.

Michael J. Hendricks et al.[13] studied the effects of seal coats on shell properties. The permeability of the mold decreased due to seal coat and there was no significant impact on strength.

2.2.5. Dewaxing. Dewaxing is generally carried out by autoclave dewaxing or flash firing. In both cases a large thermal gradient is introduced into the shells. This helps to minimize shell cracking due to wax expansion by creating a liquid layer of wax between the shell and inner wax.

2.2.6. Firing. Firing is an important stage in the process where the microstructure and properties of the shells are changed due to sintering. The process can be divided into different stages: residual wax removal, sintering and cooling. Sintering is the stage where the porous network of the shell system can be changed. Densification occurs during the process by solid state diffusion or viscous flow of material resulting in bonding of stucco and slurry particles. Densification rate is high and large reduction in porosity occurs if the shell is heated slowly to the sintering temperature[14]. It is of general practice to hold the shell isothermally, at a temperature higher than the pattern melting point, during initial stage of sintering to ensure complete pattern residue removal and rapidly heating to sintering temperature. The sintering temperature and heating rate depend on the composition of the material and the sintering parameters can be adjusted by studying a temperature density relation of that particular refractory material. Cooling of these fired

shells, generally, is done slowly to minimize cracking that might occur due to high thermal gradient.

2.3. SHELL MATERIALS

The processing steps of investment casting shells and their impact on shell properties have been discussed in the previous section. It should be noted that the processing parameters need to be adjusted according to the choice of material. It is of common practice to use different chemistries of materials for different components. The interaction between different component materials during different stages of the process and especially during the sintering process is critical for strength development of the shells. The commonly used refractory materials and binders are discussed below.

2.3.1. Refractory Materials. The common refractories used for filler and stucco are silica, aluminosilicates and zircon[3]. For fillers used in slurries, fine sized -250 mesh or -300 mesh, material is preferred to impart smooth surface to the casting. Finer stucco (-50+100 mesh) is used over the primary coat and stucco (-30+50 mesh) can be coarser in between the backup coats by which it can penetrate deep into the slurry layer providing a passage for the escaping gases.

2.3.1.1. Silica. Fused silica is the most common refractory material used for shell building. Low thermal expansion (5.5×10^{-7}/°C), chemical inertness, reduced shell weight (density of 2.2 g/cc) and ease of shell removal all make it a common choice.

The structural changes that occur in silica, during different heating cycles of the process, have to be considered. Silica is available naturally in the form of quartz. It can exist in different polymorphs all of which can be converted to other forms, depending

on temperature and pressure. The phase changes of silica with temperature and silica glass formation are shown below[15].

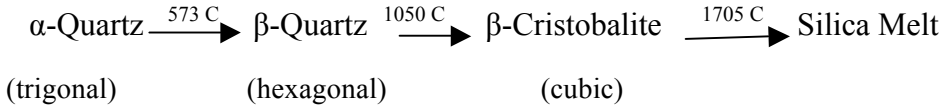

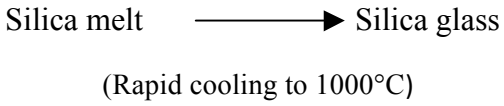

Devitrification of fused silica to β-cristobalite starts upon heating to around 1100°C. Formation of cristobalite starts from the surface of the fused silica grains and the kinetics depend on different factors such as temperature and the amount of impurities present.[16] The presence of cristobalite reduces the strength of a fused silica shell. β-cristobalite, on slow cooling converts to α- cristobalite at a temperature 270°C (low temperature form). This transformation occurs by atomic displacement resulting in the reduction of lattice volume by four percent. In an investment casting process, where fused silica shells are used, devitrification occurs depending on the temperature of the liquid metal during pouring. Formation of α- cristobalite, on cooling, generates numerous cracks in the shell due to the volume change, thus facilitating easy shell removal.

2.3.1.2 Aluminosilicates. Aluminosilicates of varying compositions are widely used in investment casting industry, mainly for backup stucco. Mullite ($3Al_2O_3.2SiO_2$) is the only stable compound between alumina and silica. Aluminosilicates are specified according to the alumina content. They are produced from fireclay raw materials that are blended, ground, extruded into pellets, calcined at a temperature around 1500°C, then crushed. This produces a mixture of mullite and dispersed silica glass.

2.3.1.3. Zircon. Zircon ($ZrSiO_4$) naturally occurs as sand, in narrow size distributions. Its high thermal conductivity (2.1 W/m.K at 25°C) offers a significant advantage over fused silica (1.3 W/m.K at 25°C). Fine zircon flour (-325 mesh) is generally used in the foundries for primary coatings. A lesser likelihood of 'burn-on' (a condition where sand gets attached to the casting degrading the surface quality) produces smooth surface finish and improves metal solidification. Since zircon is costly and relatively scarce in nature, it is generally used only for prime coats.

Feagin studied the characteristics of aluminosilicate shells.[17] He observed that the strength of shells built from Remasil 60 (80% mullite, 20% silica glass) had the highest strength (15 MPa) at 1000°C. The results showed that addition of fused silica (30% by wt.) into the slurries made from aluminosilicates lowered the strength (6.3 MPa) significantly. Since many foundries are concerned with shell removal, it is common practice in many foundries to add fused silica along with aluminosilicates.

Snow et al. did an extensive work comparing different properties of fused silica and aluminosilicate stucco.[18] Fused silica shells are observed to have high fracture toughness, least thermal expansion (0.02% linear change at 900°C) and high thermal conductivity (1.6 W/m.K at 1000°C) at high temperatures. Michael J. Hendricks et al.,[19] compared the stiffness of these shells at high temperatures and found that the fused silica shells are stiffer.

2.3.2. Binders. Binders can be classified into two categories - water based and alcohol based. Commonly used binders are silica based and various ceramics can be used for filler and stucco.

2.3.2.1. Water based colloidal silica. Colloidal silica is used as common purpose binder. It exists as aqueous colloidal silica sol. A colloid refers to a dispersion of very fine particles (1-100 nm) in a continuous liquid medium. The unique characteristic of a colloid is that it can convert from water like consistency to a jelly like substance[1]. During the drying process, silica colloids form siloxane (-Si-O-Si-) bonds between different silica particles forming silica gel. The colloids are stabilized and are dispersed throughout the liquid by carrying negative electrical repulsive charge. The electrical charges of the particles are determined by the pH of the binder. Aqueous silica binders are generally stable at pH of around 9.5 and can be stored for longer times. Contamination by any impurities from the filler changes the pH of the binder and the loose particles start linking with each other resulting in a gel. This is called sol-gel conversion. Slurries tend to have shorter life than that of binder because of introduction of impurities from outside environment. Constant monitoring and required additions to adjust the viscosity and pH can be made to help maintain a slurry for longer times (few months).

2.3.2.2. Alcohol based binder. Ethyl silicate is another compound that can be used as a binder. The common grade used in investment casting industry consists of a mixture of ethyl silicate and silica by 40% weight, designated as ethyl silicate 40.

Ethyl silicate has no binding properties. Hydrolysis results in the formation of a gel which acts as a binder. Hydrolysis is generally carried out in acidic or basic media, since ethyl silicate and water are immiscible. The hydrolysis is accelerated by addition of an acid catalyst[1]. Changing the pH of the system causes gelation and results in the formation of polymeric silica.

2.3.3. Polymer and Fiber Additions. Ceramic shells are prone to cracking during autoclave dewaxing due to different thermal expansion of the wax pattern and the mold. To increase the green strength of the mold, polymer additions to the binder is a common practice in many foundries. The polymers may be latex polymers, water-soluble polymers or their mixtures. Suitable latex polymers include vinyl acetates, polyvinyl chlorides, acrylics and styrene butadienes. Water-soluble polymers can be polyvinyl alcohols and various cellulose ethers. Organic fibers can also be added to modify the strength and performance of the shell. These organic, water-insoluble fibers are dispersed in the slurry and their dimensions determine the behavior of the coatings.

Many works have been carried out to compare the performance of polymer and fiber modified shells.[20, 21] The experiments done by Jones et al.,[21] compared properties two sets of shell; polymer modified (6 wt % of binder was used in primary slurry, 8 wt% in back-up slurries) and fiber modified shells (20g/Liter of binder liquids, only in back-up coats). It was determined that polymer modified shells were stronger (7.8 MPa) in green condition when compared to fiber modified shells (4.7 MPa). There was no variation observed in the fired strengths (4.8 MPa) of these shells. Hot permeability (800°C) for fiber modified shells was three times that of polymer modified shells.

Another important characteristic of fiber addition is that the thickness of the shell increased by 15% when compared to polymer modified shell.[21] This enhances the load bearing capacity of weaker edges of the mold which can help against shell cracking during pattern removal.

2.4. FRACTURE OF POROUS CERAMICS

Investment casting shells are layered ceramic structures, where each layer has a slurry coating on which stucco is applied and allowed to dry before the next coating. The presence of stucco between the slurry layers results in porosity. A typical polished cross section of an investment casting shell is shown in Figure 2.1. Depending on various process parameters, the cross section can have a layered structure, a monolithic structure or a combination of both[12]. The overall fabrication process of the shells makes the cross-section of the shell complicated and a clear analysis of the microstructure is required to explain different factors that control the fracture strength of the shells.

Ceramics fail by brittle fracture that is controlled by the presence and distribution of microstructural flaws like large pores, coarse grains, second phase particles or flaw clusters. The effect of porosity and other microstructural variations on the fracture of investment casting shells can be understood by studying the impact of microstructure in different classes of ceramics and comparing these to microstructural features of the shell.

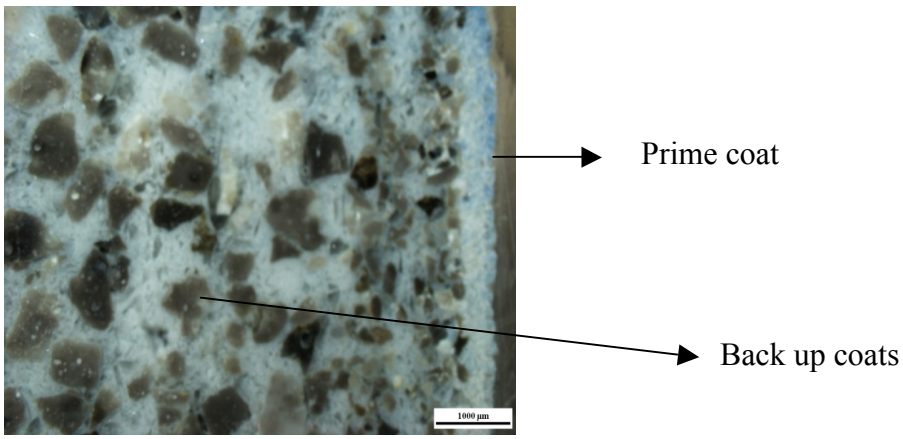

Figure 2.1. A typical polished cross section of shell

The occurrence of porosity and microcrack formation during the fabrication and processing of the shells are the weak links that control the fracture of the shells. Porosity is relatively higher in the stucco layer than it is in the matrix formed from slurry. The fabrication of shells involves coating a pattern and stuccoing it alternately. Depending on the size and shape of stucco and slurry parameters, porosity arises when the entrapped air between previous stucco layers did not escape through the slurry coating. Microcracks arise due to mismatch in thermal expansion or differential diffusion between different phases or grains, during sintering, of the shell.

Sintering, by which a broad range of microstructures can be produced, has to be considered to study ceramic properties. Sintering is a densification process where the porosity and grain size change depending upon the time and temperature of the process. In general, grain growth occurs and porosity decreases in sintering.[22]

Porosity effects on mechanical properties of different classes of ceramics, processed by different methods, have been studied extensively. Roy W. Rice evaluated the dependence of strength on porosity based on minimum solid contact area model (MSA) and proposed a simple equation (equation 1) for strength of porous ceramics.[22] This equation indicates that strength (σ) decreases as volume percent porosity (P) increases.

$$\sigma = \sigma_0 \exp(-bP) \tag{1}$$

In the above equation, σ_0 is the strength of the fully dense material and b is the empirical parameter related to the minimum solid area and pore structure.

Coble and Kingery[23] studied the effect of varying amounts of porosity on the properties of sintered alumina, prepared by slip casting. Figure 2.2 shows the polished cross sections of sintered porous alumina. The strength decreased with increased porosity, predicted by equation 1.

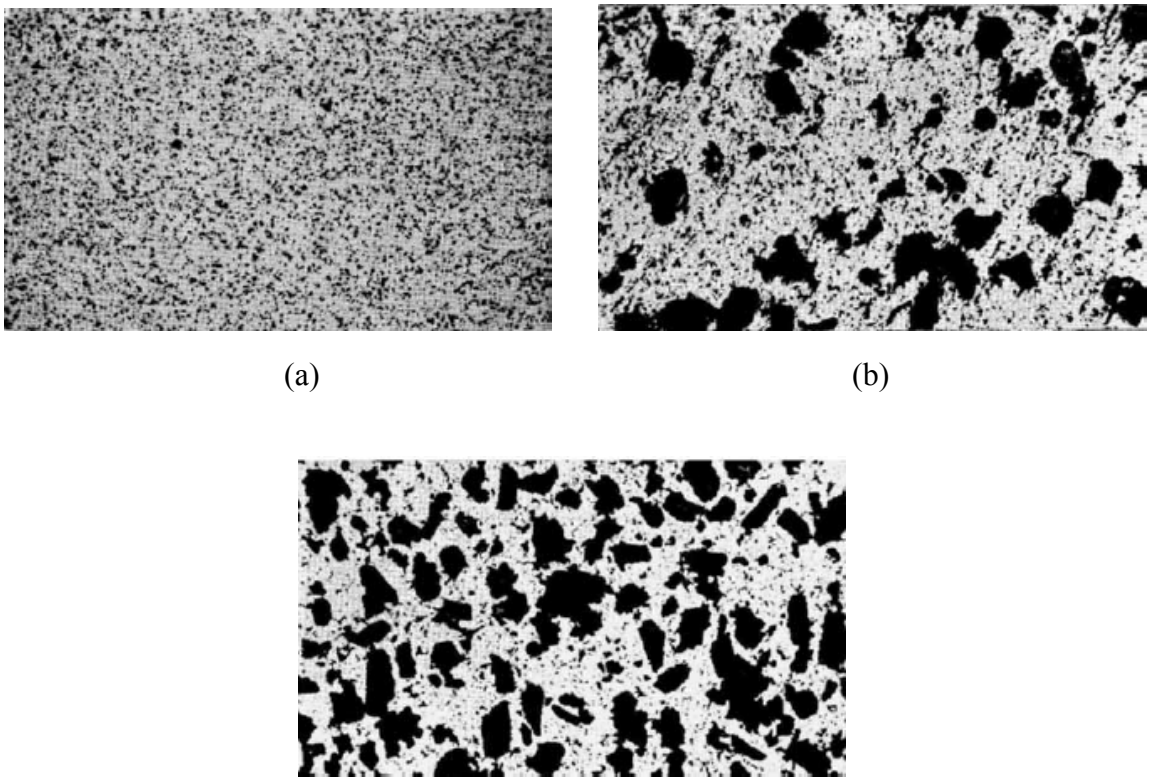

(a) (b)

(c)

Figure 2.2: Polished cross sections (50X) of alumina having (a) 8% (b) 20% (c) 37% porosity.

Coronel et al. studied the sintering behavior of glass microspheres.[24] They analyzed the microstructure and mechanical behavior of sintered glass having different densities. The rupture stress increased (10 MPa to 30 MPa) with relative density (0.6 to 0.9) and the fracture toughness measured reached a maximum and then decreased at high

densities ($\rho > 0.85$). The authors explained this trend of fracture toughness with reference to microstructual changes that occur in sintering (Figure 2.3). The densification mechanism of spheres occurred by viscous flow and at low relative densities (up to 0.75) fracture toughness increases because of the increased crack path due to strengthening occurred by the neck growth of spheres. At high densities ($\rho > 0.85$) the microstructure is observed as a bulk containing isolated pores that acts as crack growth inhibitors. Hence there would be little strain (0.2%) and fracture toughness decreases with increase in density.

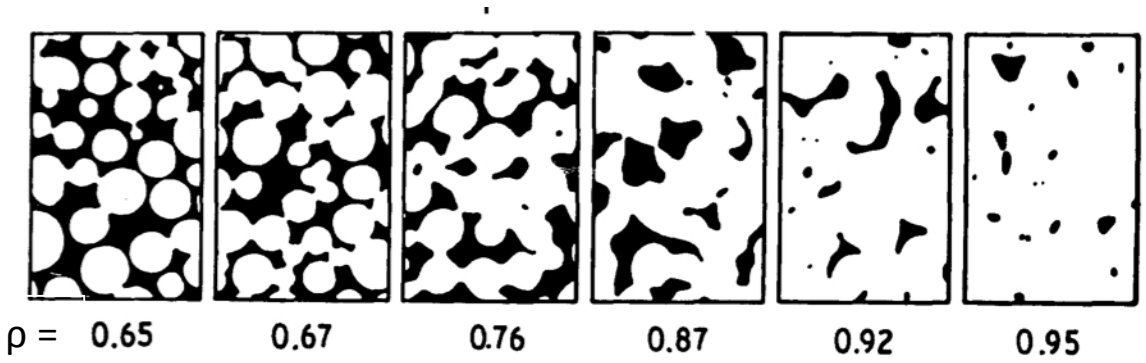

Figure 2.3. Changes in pore network as the relative density (ρ) increases during sintering[24]

In addition to the fracture behavior of single-phase ceramics, studying the properties of particulate ceramic composites can help for a better understanding of fracture of investment casting shells.

The incorporation of particulates in a ceramic matrix affects the sintering behavior of the composite. The main differences arise due to mismatch in diffusion coefficients and thermal expansion coefficients of particulate and matrix phases[25]. When the two phases have similar diffusion coefficients, sintering behavior is enhanced because the particles are mobile and coalescence occurs easily. When the difference between the

diffusion coefficients is high, the particles in one of the phases at the interface may not move easily and the coalescence might not occur. Thermal expansion mismatch results in residual micro-stresses. The higher thermal expansion of the particle results in tensile residual stresses in the surrounding matrix. Effectively the material at the interface around the particle is weakened and the cracks are attracted towards the matrix. In the other case when the particle matrix interface is strong, the crack is attracted towards the particles. Figure 2.4 shows the crack paths of two different composites. In Figure 2.4(a), when there is strong interface, (TiN/Al_2O_3 interface) strength is enhanced and the crack path is through the matrix and particles and when there is weak interface crack is only through the matrix (Cr_3C_2/Al_2O_3 interface).

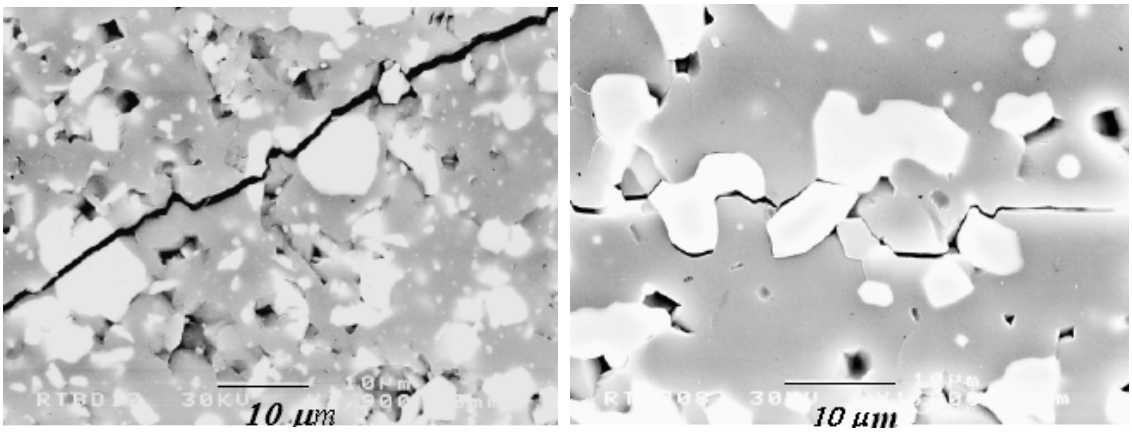

(a) (b)

Figure 2.4[26]: Crack paths in alumina matrix composites containing 20 vol% of (a) TiN particles (b) Cr_3C_2 particles

The fracture behavior of investment casting shells depends on both porosity and the interaction between stucco and slurry matrix during sintering. A careful consideration of different parameters affecting pore size and sintering behavior of different phases of

different particle sizes can help in identifying the controlling factor for shell strength. A qualitative and quantitative microstructural analysis is required to understand the mechanical properties of investment casting shells.

2.5.FOCUS OF RESEARCH

The objective of this research was to analyze the effects of both raw material properties and process parameters on the properties of investment casting shells. Material properties considered for this study were chemistry, type of additions, particle size and particle size distribution. There are many process parameters that could affect the shell properties; for studying strength of the shells, parameters that affect the material (stucco or slurry) uptake, are critical. Hence parameters such as slurry viscosity, pattern dipping time and stuccoing time were considered.

The interaction between slurry and stucco, at different processing stages resulting in porosity variations was studied by measuring the strength of the shell in different conditions – green, fired and cooled, and hot. The shells were additionally characterized for microstructure to observe the distribution of stucco grains in the matrix and the distribution of porosity.

3. EXPERIMENTAL PROCEDURES

3.1. RAW MATERIALS

3.1.1 Material Selection. Different raw materials were chosen to analyze the effects of individual components - flour, binder or stucco - on shell properties. From a list of most commonly used and commercially available investment casting supplies, different raw materials were selected as listed in Table 3.1.

Table 3.1. Different flours used for this study

	Material	Supplier	Description
1	Ranco-Sil # 1	Ransom & Randolph	Fused silica with narrow particle size distribution, (-325 mesh)
2	Ranco-Sil # 4	Ransom & Randolph	Fused silica with wide particle size distribution, (-200 mesh)
3	Gray Matter	NALCO	Predominantly fused silica with polyisopropylene fiber additives
5	REMASIL	REMET	Fine aluminosilicate powder with 70% alumina, (-325 mesh)

Table 3.2. Different types of stucco used

	Material	Supplier	Description
1	Ranco-Sil	Ransom & Randolph	Fused silica stucco
2	M70	Ransom & Randolph	Aluminosilicate stucco with 70% alumina

Table 3.3: Different types of binders used and their properties

	Material	Supplier	Average particle size, nm	Silica, wt%	Na_2O, wt%	Surface area, m^2/g
1	Megasol	Wesbond	70 (polydispersoid)	50	0.22	70
2	Nalco 1030	NALCO	13 (monodispersoid)	30	0.50	230
3	Nalco 1115	NALCO	4 (monodispersoid)	15	0.75	750
4	Megasol + ESP 6305 (polymer)	Wesbond + NALCO	Megasol + 6 wt% polymer			

Two chemistries of refractories were considered: fused silica and mullite. Flours had varying particle size distributions in addition to chemistry. Binders differed in average particle size and stuccos differed in chemistry. External additives like fibers or polymer were also considered.

3.1.2. Flour Characterization. Refractory flours were characterized for chemical composition and particle size distribution using the following techniques:

Particle size distributions (PSD) of flours were measured based on the principle of laser scattering. Particle analyzer S3500 (Microtrac, USA) was used for this. A small amount of powder, 1 or 2 mg, was suspended in flowing deionized water. Laser beam (wavelength 780 nm) was scattered by the individual particles and the particle size data was obtained. Sampling a small amount of material, 2 mg, for this analysis from bulk (50 lb bag) was a major concern. Sampling riffle splitter was used to sample a small amount of material, of about 1 g, and analysis was done on multiple samples.

Electron Microscopy was used to characterize the geometry of particles in refractory powders. Scanning electron microscope, ASPEX 1020 (Aspex Corporation,

USA), was used for this. The powders were sieved to different size ranges and imaged. The back-scattered images were acquired for each of these powders.

Figure 3.1 shows the particle size distribution by volume for Ranco-Sil # 1. The histograms show the differential percentage of the corresponding size and the error bars show the variation during multiple analyses. The curve indicates the average of cumulative percentage of particles under corresponding sizes. It was observed that Ranco-Sil # 1 had a relatively narrow distribution (0.5 - 75 μm) and the error bars were small. The milled product has a distribution that is log normal, so a bell shaped continuous curve would be obtained. The gap in the distribution may be due to the addition of fine fused silica (0.5 - 2 μm) powder, which would enhance the surface finish of the casting.

Figure 3.2 is a micrograph of the structure of Ranco-Sil # 1. The sample analyzed had been sieved to -270 mesh. The particles were observed to be non-spherical in shape with numerous aspect ratios as well as geometries.

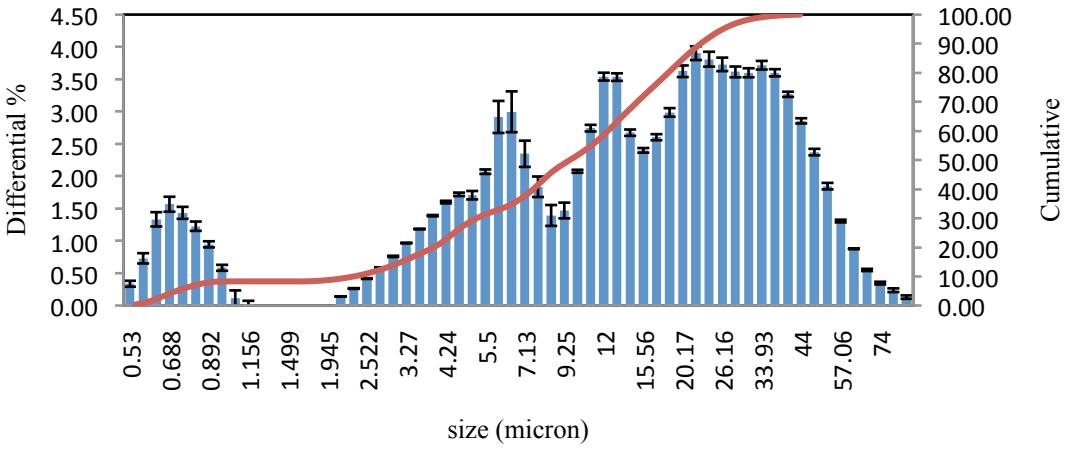

Figure 3.1: Particle size distribution (by volume) plot for Ranco-Sil # 1

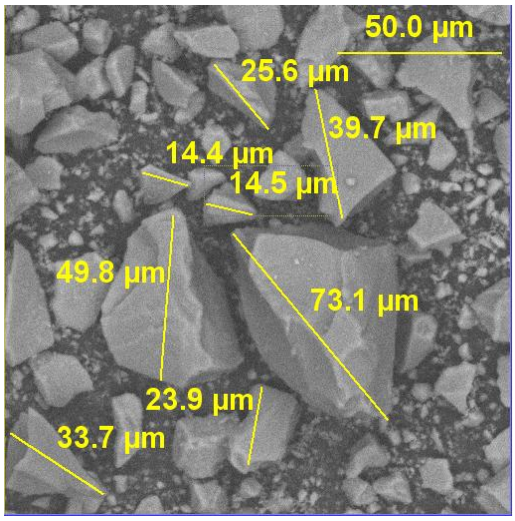

Figure 3.2: Microstructure of particles in Ranco-Sil # 1

Ranco-Sil # 4 was observed to have a wider distribution (0.5 - 300 µm) and large error bars, which show the variation in multiple samples (Figure 3.3). A similar gap in the distribution, as seen in Ranco-Sil # 1, was observed for this material as well.

A sample of Ranco-Sil # 4 was divided into three different size ranges by sieving and was observed for microstructures. The geometries of the particles were observed to be similar to that of Ranco-Sil # 1. Figure 3.4 is a micrograph showing the geometries of different particles of Ranco-Sil # 4.

Gray Matter is the name used to describe a predominantly fused silica flour, containing polyisopropylene fibers. It has a wide size distribution (0.5 - 400 µm) and the variation in multiple samples is also very high (Figure 3.5). The smaller percentage (< 1%) of material between 0.5 µm and 3 µm may be due to the presence fibers in the sample. Figure 3.6 shows the micrograph of the particles in Gray Matter. The wide size range (10 µm – 900 µm) of the particles is indicated.

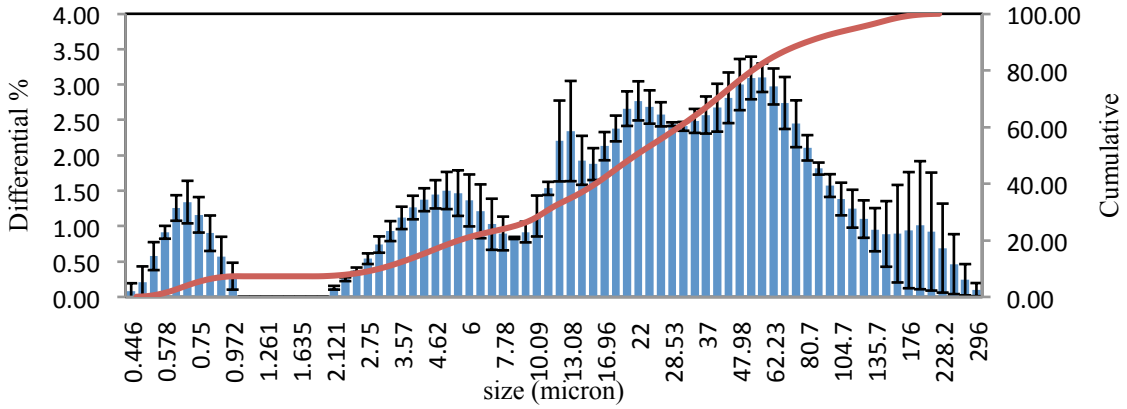

Figure 3.3: Particle size distribution (by volume) plot for Ranco-Sil # 4

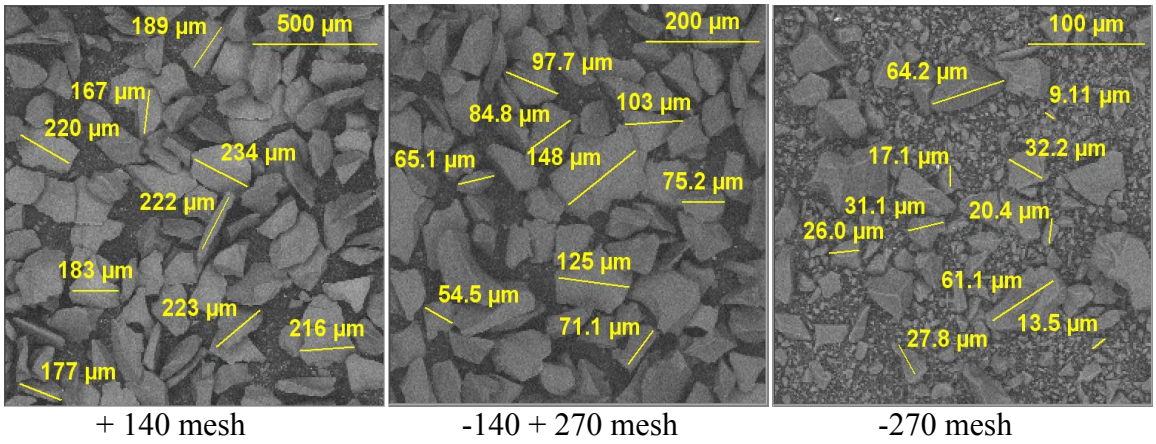

Figure 3.4: Microstructure of particles in Ranco-Sil # 4

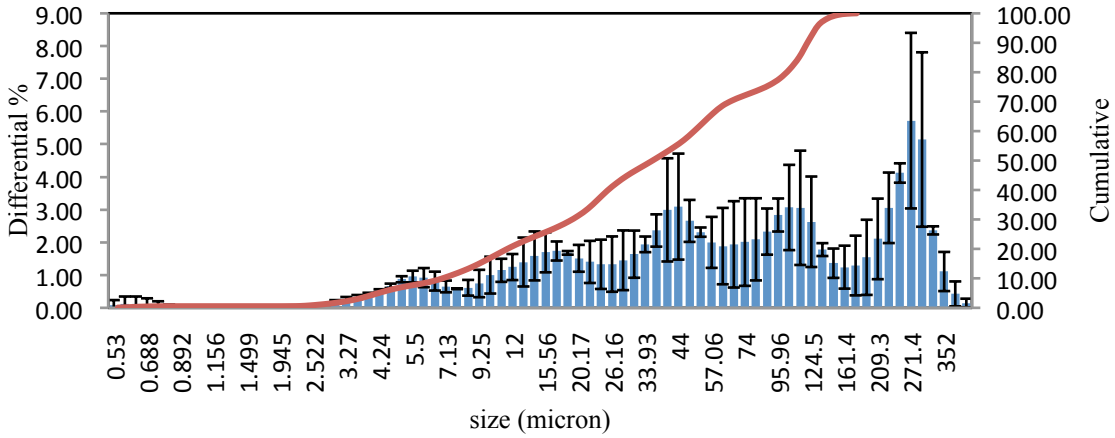

Figure 3.5: Particle size distribution (by volume) plot for Gray Matter

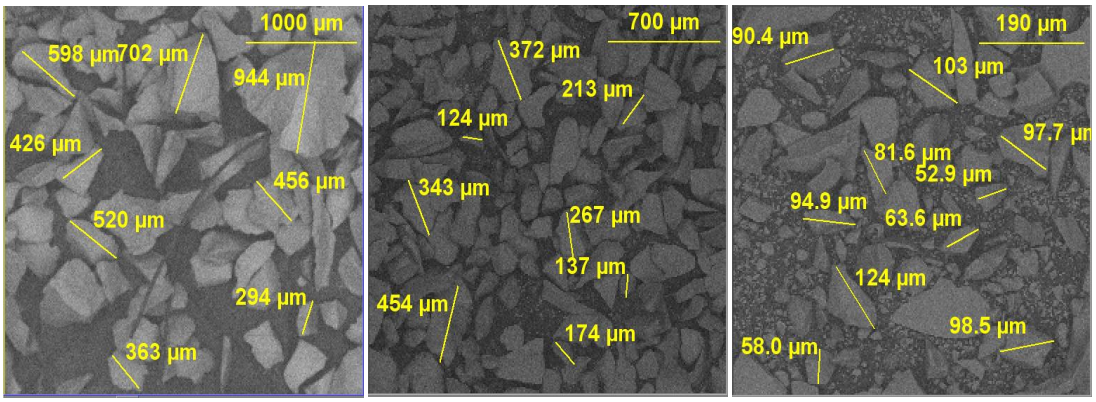

+70 mesh -70 +140 mesh -270 mesh

Figure 3.6: Microstructure of particles in Gray Matter

Remasil is aluminosilicate flour with a total alumina content of 70%. The particle size distribution (Figure 3.7) is observed to be a bell shaped curve. The microstructure of the powder (Figure 3.8) suggests that the particles are angular as observed with fused silica flours.

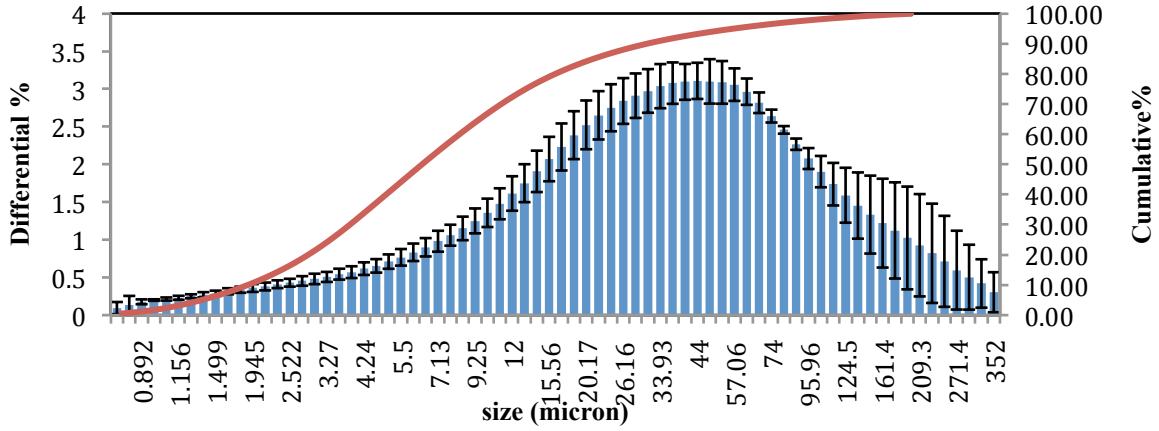

Figure 3.7: Particle size distribution (by volume) of Remasil flour

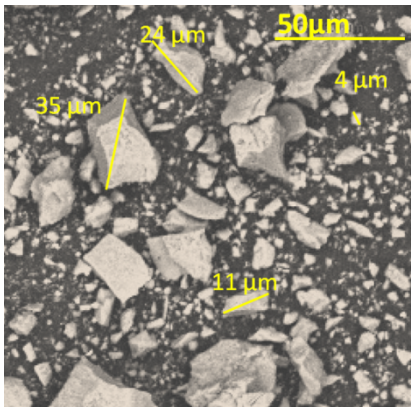

Figure 3.8: Microstructure of Remasil powder

Table 3.4 compares the particle size distribution for different flours by citing three values d_{10}, d_{50} and d_{90}. d_{10} represents the particle size below which 10% of the material lies. Similarly, 50% of the material lies below d_{50} and 90% below d_{90}.

Table 3.4: Comparison of particle size distributions of different flours

Flour	d_{10}, µm	d_{50}, µm	d_{90}, µm
Ranco-Sil # 1	3	15	40
Ranco-Sil # 4	3	26	104
Gray Matter	10	67	270
Remasil	2	9	50

X-Ray diffraction (XRD) was performed on powders to determine the phase(s) present. Ranco-Sil # 1 was observed to be completely amorphous. The XRD pattern of Ranco-Sil # 4 showed some traces of quartz (Figure 3.9). Gray Matter has proprietary crystalline additives and is predominantly fused silica flour. The XRD results (Figure 3.10) indicate the presence of mullite with fused silica.

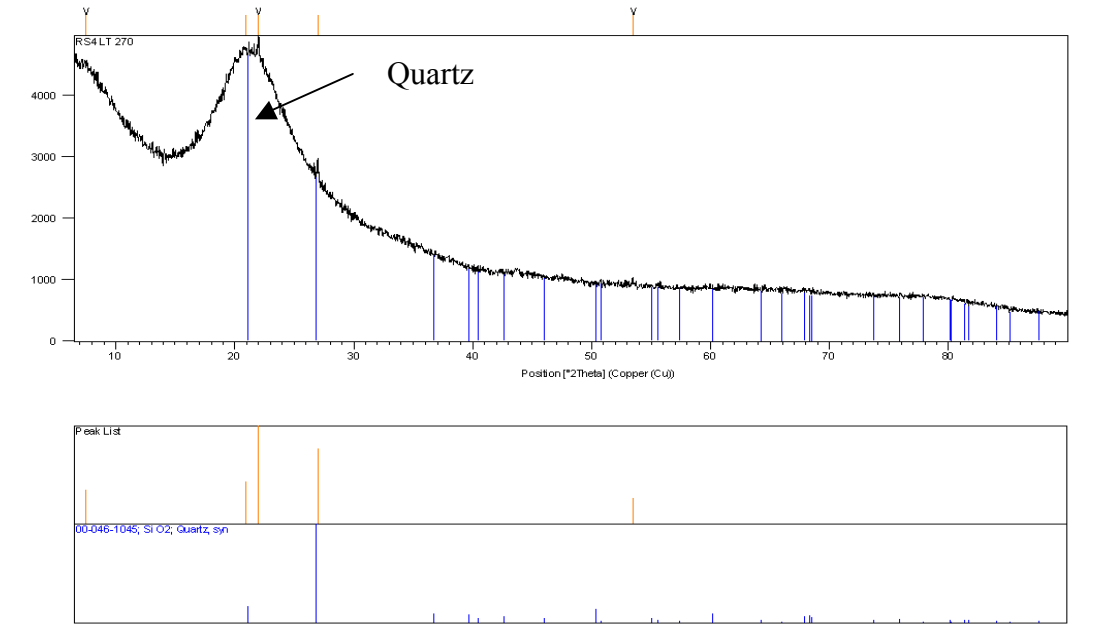

Figure 3.9: XRD pattern of Ranco-Sil # 4 showing traces of quartz.

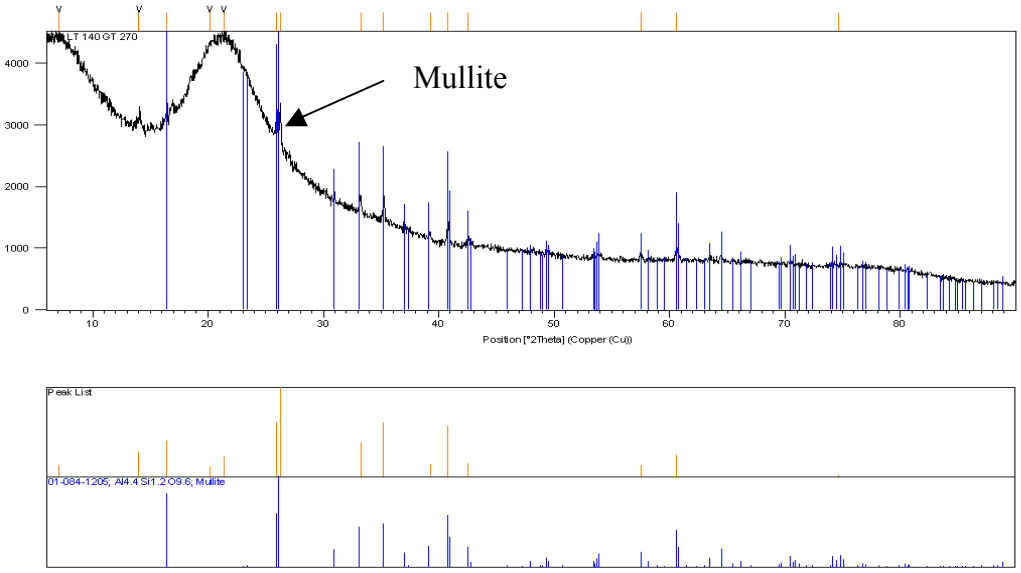

Figure 3.10: XRD pattern of Gray Matter showing presence of mullite

The specific surface area of the powders was measured by BET (Brunauer Emmett Teller) method using NOVA 2000e Surface Area Analyzer (Quantachrome

Instruments, USA). BET method is based on adsorption of gas molecules on the surface of powder particles by which surface area is determined. The surface area measured for different flours is presented in Table 3.5.

Table 3.5: Specific surface area of refractory flours

	Specific surface area (m^2/g)
Ranco-Sil # 1	10.01
Ranco-Sil # 4	7.65
Zircon	7.45
Remasil	8.17
Gray Matter	10.16

3.1.3. Stucco Characterization. Two types of stucco, Ranco-Sil and M70, were characterized for size and shape analysis. Finer stucco (-50+100 mesh) was used for primary and first back-up coats while coarse stucco (-30+50 mesh) was used for rest of the back-up coats. The images of these powders, as observed from scanning electron microscope, are shown in Figures 3.11 and 3.12. Fused silica stucco (Ranco-Sil) particles were relatively more angular when compared to aluminosilicate stucco (M70).

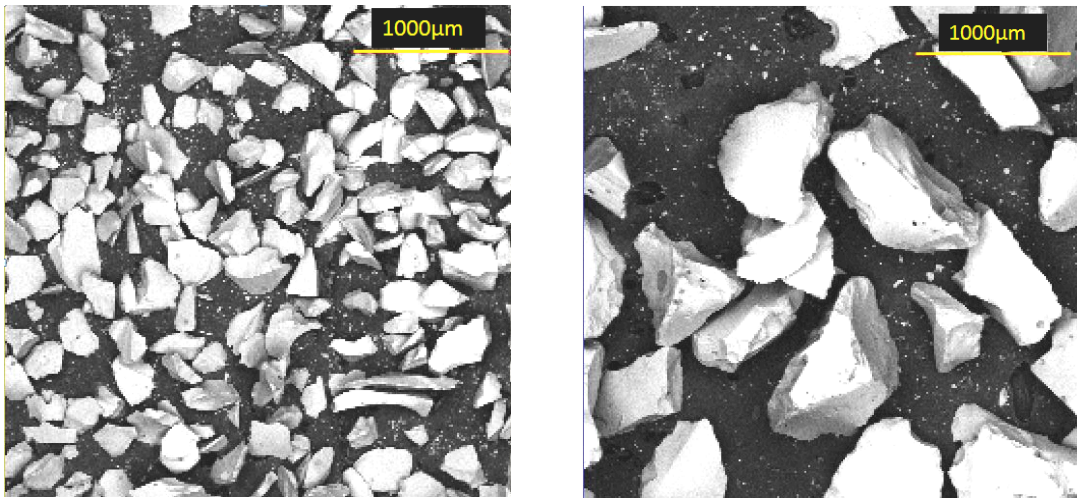

(a) -50+100 mesh (b) -30+50 mesh

Figure 3.11. Microstructure of Ranco-Sil stucco (a) -50+100 mesh (b) -30+50 mesh

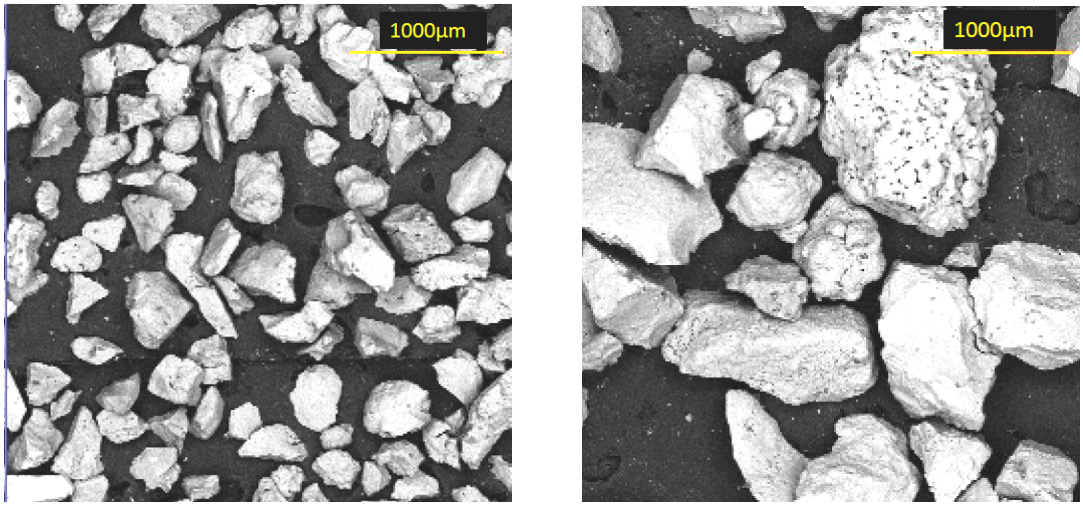

(a) -50+100 mesh (b) -30+50 mesh

Figure 3.12. Microstructure of M70 stucco (a) -50+100 mesh (b) -30+50 mesh

3.2 DESIGN OF EXPERIMENTS

To understand the effect of flour, binder and stucco characteristics on the properties of shells, the individual behavior and the interaction between different components during the fabrication and post processing of the shells were investigated. A set of experiments was designed, where shell systems were made using different combinations of raw materials as listed in Table 3.6.

Table 3.6: Design of experiments for evaluating the material effects on shell properties

System	Batch	Prime coat		Back-up coats		Stucco
		Flour	Binder	Flour	Binder	
1	A	Ranco-Sil # 4	Megasol	Ranco-Sil # 4	Megasol	Ranco-Sil
	B	Ranco-Sil # 4	Megasol	Ranco-Sil # 4	Megasol	M70
2	A	Remasil	Megasol	Remasil	Megasol	Ranco-Sil
	B	Remasil	Megasol	Remasil	Megasol	M70
3	A	Ranco-Sil # 1	Megasol	Ranco-Sil # 1	Megasol	Ranco-Sil
	B	Ranco-Sil # 1	Megasol	Ranco-Sil # 1	Megasol	M70
4	A	Zircon	Megasol	Gray Matter	Megasol	Ranco-Sil
	B	Zircon	Megasol	Gray Matter	Megasol	M70
5		Ranco-Sil # 4	Nalco 1030	Ranco-Sil # 4	Nalco 1030	Ranco-Sil
6		Ranco-Sil # 4	Nalco 1115	Ranco-Sil # 4	Nalco 1115	Ranco-Sil
7		Ranco-Sil # 4	Megasol + ESP 6305 (polymer)	Ranco-Sil # 4	Megasol + ESP 6305 (polymer)	Ranco-Sil

Another set of experiments was aimed at control of the shell building process. Since the process of shell building involves multiple stages that extend over a period of 2-3 days, the process parameters at different stages have to be carefully monitored to provide a homogeneous and consistent shell build. The properties of the shell are mainly affected by material uptake during pattern dipping and stuccoing. The effects of slurry viscosity and stucco size were studied by analyzing the shell microstructures. The effects of dipping time and stuccoing time were studied by determining the changes in the amount of slurry/stucco additions with varying dipping/stuccoing times. Table 3.7 and 3.8 summarizes the shell building parameters chosen for this study. For shell systems in Tables 3.7 and 3.8, Ranco-Sil # 4 was used as flour, Megasol as binder and Ranco-Sil as stucco.

Table 3.7: Process parameters used to study shell microstructures

System	Slurry viscosity, cP	Stucco size
1	700-800	-30+50 mesh
2	700-800	-50+100 mesh
3	300-400	-30+50 mesh
4	300-400	-50+100 mesh

Table 3.8: Process parameters used to study the variations in material additions

System	Stucco size	Dipping time, sec	Stuccoing time, sec	Slurry viscosity, cP
1	-30+50 mesh	10	20	600-700
2		20		
3		30		
4	-50+100 mesh	20	10	
5			20	
6			30	

3.3. SHELL BUILDING PROCESS

All shells prepared for this study had one primary coat followed by five back-up coatings. Each coating is allowed to dry for a minimum of four hours. No seal coat was applied to the shells.

3.3.1. Pattern Making. Expanded Polystyrene Sheets (EPS) were used to make patterns. Two geometries of patterns were made: (i) rectangular, 5’’x 3’’x 1’’ (ii) 3’’ thick wedge shape patterns with face geometry as shown in Figure 3.13. The wedge shape patterns were further machined on edge AD to a radius of 5mm.

Sheets of EPS have very little texture. To improve adhesion of slurry to the pattern surface, all patterns were polished uniformly with 180-grit sand paper, before shell fabrication.

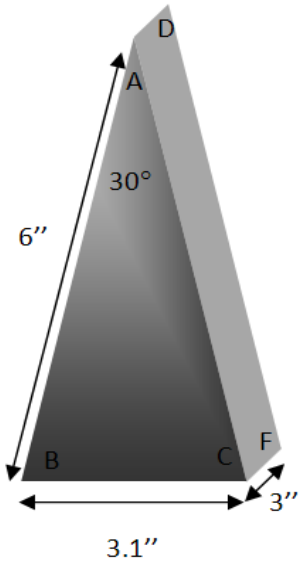

Figure 3.13. Geometry of wedge specimen

3.3.2. Slurry Characteristics. Slurry parameters typically employed in foundries were determined. For all shell systems in initial design of experiments, parameters shown in Table 3.9 are used. High viscosity (1000 cP) and high filling ratio (wt. of binder/wt. of flour) for primary coat is generally preferred to provide smooth surface finish to the casting.

Table 3.9: Slurry characteristics

Slurry		Primary coat		Back-up coats	
Binder	Flour	Filling ratio	Viscosity range (cP)	Filling ratio	Viscosity range (cP)
Colloidal Silica	Fused Silica	2.5:1	900-1000	2:1	350-450
	Mullite	3:1		2.5:1	
	Zircon	4:1			

3.3.3. Slurry Preparation. The setup used for slurry making is shown in Figure 3.14. Binder and other liquid additives were poured into the bucket and weighed. Flour was then added slowly into the bucket as per the required ratio and the initial high shear mixing was done by a mixing rod attached to a 330 RPM/40 HP motor. Once the binder and flour were mixed thoroughly and homogeneously, the bucket was placed on a plate rotating at 15 RPM. An ‘L’ shaped rod was inserted to prevent the solids from settling down. When compared to conventional mixing equipment, this type of setup prevents the formation of vortex and hence reduces the amount of entrapped air in the slurry.

Figure 3.14. Setup for slurry mixing

The viscosity of slurry was adjusted by addition of distilled water. Brookfield DVII Pro viscometer (Brookfield Engineering Laboratories, USA) was used to measure slurry viscosity. The viscosity was measured and maintained in the required range throughout the process.

3.3.4. Pattern Coating, Stuccoing and Drying. The patterns were dipped in slurry for about 15 sec, taken out and the pattern was held out to allow the slurry to drain out. While the slurry drained out, the pattern was being rotated slowly to maintain a uniform coating all over the geometry of the pattern.

For the second design of experiments, the dipping time and draining time were controlled and monitored by a stopwatch. The weight of slurry added was recorded when draining was stopped.

Stucco was applied over the patterns using rain-fall sander shown in Figure 3.15. While the stucco fell on the pattern, it was rotated to ensure uniformity. The weight of stucco added was recorded in the required shell systems. Fine stucco, -50+100 mesh, was used on prime coat and the immediate backup coat to avoid penetration of stucco into the

slurry layer. Coarser stucco, -30+50 mesh, is used for the backup coats. The shells, after each coating, are air-dried in the presence of dehumidifier for a minimum of four hours.

Figure 3.15. Rainfall Sander

3.3.5. Pattern Removal and Firing. To avoid any shell cracking due to stresses developed by thermal expansion of patterns during firing, the EPS patterns were removed from the shells before the firing process. Acetone was used to dissolve the EPS foam. During firing, the shells were cut into required test piece sizes, heated up to 800°C, where they were held for two hours, and were furnace-cooled back to room temperature.

3.4. SHELL TESTING

3.4.1. Strength of Shell. Strength of investment casting shells is generally evaluated by measuring flexural strength, also called as Modulus of Rupture (MOR). It is the stress at fracture of the shell and can be measured by three-point bend test.

$$\sigma_f = {}^{3Pl}\!/_{2bd^2} \tag{2}$$

In the above equation, σ_f is the flexural strength or MOR, P is the load at failure, l is the span length between supporting points, b is the width of the sample, and d is the thickness.

Figure 3.16 shows the setup of eXpert 5602 Universal Testing Apparatus (ADMET, USA) used for three-point bend test. A test piece is rested on two stationary points and load is applied on the opposite face at the centre line till it fails. MOR is intrinsic property of the material and hence independent of dimensions. However, all shells tested had fixed dimensions ($l = 7\ cm$ and $b = 3\ cm$). The machine was controlled such that the loading block or rod moves downwards at a rate of 0.2 mm/s during the test.

Figure 3.16. ADMET Universal Testing Apparatus for three-point bend test

When liquid metal is poured into the mold, the surface of the shell in contact with hot metal is exposed to high temperature and hence is under tension. The other face is under compression. To resemble similar conditions in the testing of investment casting shells, the primary surface was rested on stationary points and the load was applied on the other face.

Flexural strength for all shell systems was measured in three different conditions: at room temperature, fired and cooled back to room temperature, and at hot temperature of 1100°C. For testing at high temperature a separate furnace is setup (Figure 3.17 and 3.18) at Missouri S&T.

Figure 3.17. Furnace chamber attached to ADMET machine for high temperature testing

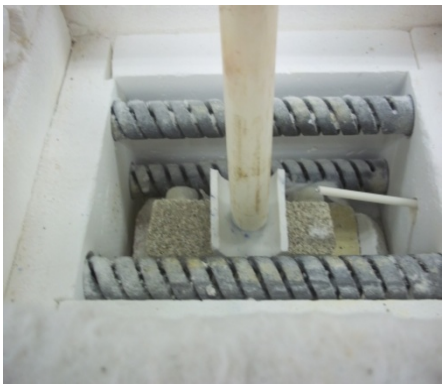

Figure 3.18. Sample setup inside the furnace chamber

In addition to MOR testing, edge strength of the shells was also analyzed. Shells were made on wedge patterns of geometry shown in Figure 3.13. Test pieces were cut as shown in Figure 3.19 and were tested for strength. A wedge block exerted force on the shell till it broke. The schematic of the test and the geometrical parameters are shown in Figure 3.20. Wedge test was performed on the shells in two conditions: green and fired. The strength (σ) of the wedge pieces was calculated form Hyde's equation (equation 4).

$$\sigma = 12.2\frac{\sin\theta\cos\theta Fd}{wt^2} \tag{3}$$

Here, F is the load at fracture, w is the width of the test piece, t is the thickness of the shell, d is the loading distance and θ is the angle of the wedge block as indicated in Figure 3.20.

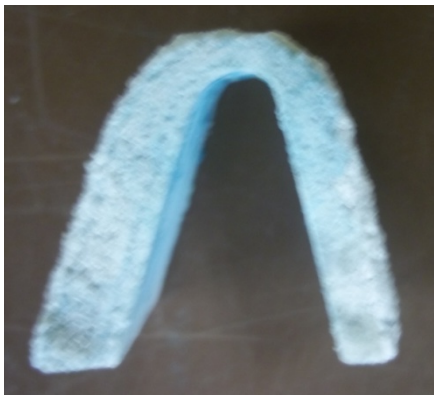

Figure 3.19. Shell test piece for wedge strength testing

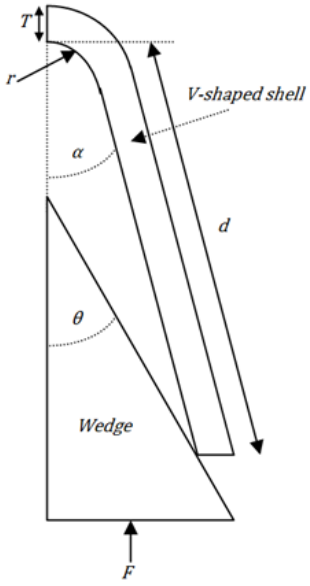

Figure 3.20. Schematic of a wedge test

3.4.2. Porosity. Apparent porosity of the shells was measured according to ASTM C20, based on Archimedes principle. Small rectangular pieces of fired shells were used to measure the porosity. The shell was first heated to 120°C to ensure that complete evaporation of moisture takes place. Its weight was measured (W_1). Then with the support

of thin copper wire, it was submerged completely in water. To achieve better penetration of water into the pores, the water container was heated on a hot plate. The water was allowed to boil for one hour and left to cool back to room temperature. Then weight of the sample in water was noted (W_2). The wet sample along with the wire was taken out and the wire was carefully removed. Any water on the surface of the sample was removed by gently wiping the surface with a piece of paper. The weight (W_3) of the shell sample with water inside the accessible pores was noted. Equation 5 was used to measure the apparent porosity (P) of the shells.

$$P = \frac{W_3 - W_1}{W_3 - W_2} \tag{4}$$

3.4.3. Permeability. Permeability of the shells was measured using Simpson-Gerosa Digital Absolute Permmeter (Simpson Technologies Corporation, USA). Samples for permeability testing were prepared by attaching discs of shells to the ends of plastic tubes (internal diameter = 2'') using silicone adhesive. The cross section of the shell was also covered with silicone to make sure that no air escapes through cross section. A typical test piece is shown in Figure 3.21. The test piece was attached to the permmeter as shown in Figure 3.22. Here air at a constant pressure (10 g/cm^2) was allowed to go out through the shell. AFS permeability number ($Perm_{AFS}$) was displayed when all the air was expelled. Darcy Permeability (k_D) was calculated using the equations (5 and 6) shown below.

$$k_D = \frac{V}{t} \cdot \frac{\mu}{A} \cdot \frac{L}{\Delta P} \tag{5}$$

$$t = \frac{763.94}{Perm_{AFS}} \tag{6}$$

Here, V is the volume of air passed through the sample, t is the time, ΔP is the difference in air pressure inside and outside the sample, μ is the viscosity of air at 25°C, A is the internal surface area of the sample, and L is the average thickness of the sample.

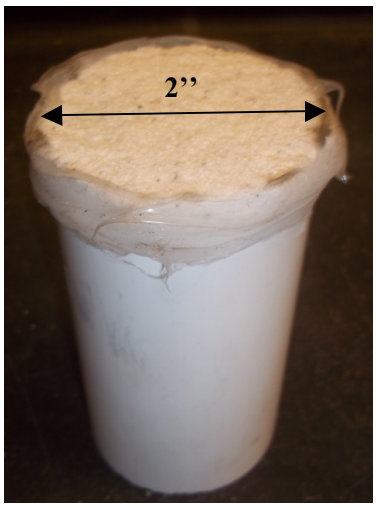

Figure 3.21: Shell attached to plastic pipe with silicone for permeability testing

Figure 3.22. Digital Absolute Permmeter used to measure permeability

3.5. MICROSCOPY OF INVESTMENT CASTING SHELLS

The interaction between individual components of the shell was studied by observing the polished cross section of the shell with scanning electron microscope.

3.5.1. Sample Preparation. Samples were cut from the fired shells and were impregnated with low viscosity epoxy under vacuum so that the accessible porosity was filled with epoxy and grain pullout could be minimized during subsequent grinding and polishing. For this, EpoThin® Epoxy Resin and EpoThin® Epoxy Hardener are mixed in specified ratio. The mixture was warmed up and was allowed to impregnate into the shell samples in a vacuum chamber. The samples were taken out after curing for a day and were ground using diamond grit discs. The grinding and polishing procedure is mentioned below in Table 3.8.

Table 3.10: Polishing procedure for ceramic shell samples

Rough grinding	Diamond toothed wheel (to remove surface epoxy layer) followed by 80 grit size diamond wheel
Polishing	Diamond discs - 125µm, 75µm, 45µm, 15µm, 3µm
Fine polishing	Diamond paste solution on a cloth - 3µm, 1µm, 0.5µm

3.5.2 Microscopy. For the initial microscopic observation, optical microscope was used to study the distribution of stucco, porosity and the matrix formed from the slurry. It was observed that the contrast between glassy phases like fused silica and the epoxy was poor in the images from optical microscope. Hence scanning electron microscope, ASPEX 1020 (Aspex Corporation, USA), was used to obtain back-scattered electron diffraction (BSE) images. The samples for electron microscope observation were

prepared by first etching the polished samples using concentrated HCl for 10 minutes followed by gold coating to make the surface conducting. Etching of the shells using concentrated HCl helps in clearly identifying the boundary between the stucco and matrix. Quantitative image analysis was done using ImageJ (Java-based image processing software developed by National Institutes of Health, USA). The relative amounts of different constituents were determined and related to the strength of the shells.

4. MATERIAL EFFECTS ON SHELL PROPERTIES

Various shell systems were prepared, according to the design of experiments described in Table 3.3, to study the effects of raw material properties. Shells and the test pieces were prepared following the procedures explained in the previous section.

4.1 MECHANICAL STABILITY OF THE SHELL SYSTEMS

The mechanical stability of shells was evaluated by measuring MOR in a three-point bend test configuration. The results were categorized on material variables and summarized below. In the following plots, the labels on the horizontal axes indicate the material variable of the shell system and the vertical axis measures MOR in MPa. The error associated with the data point indicates the respective standard deviation calculated from the measurement of MOR for three different shells within the same shell system.

4.1.1. Green Strength. The shells prepared were allowed to dry for a day and test pieces were prepared. Green strength was measured for the shells at room temperature after drying and before firing.

4.1.1.1. Effect of flour properties on green strength. The chemical composition and particle size distribution of flours were considered in this study. The effects of these variables on green strength are shown in Figures 4.1 and 4.2 respectively. All shells considered for this study had Megasol as binder and Ranco-Sil (fused silica) as stucco.

The green strength of a shell is generally dependant only on the gel forming behavior of the binder used in the slurry.[7] Gelation of the binder occurs upon drying, forming a continuous network amorphous silica particles which holds the flour and stucco together. Hence green strength depends on the strength of the network. All the

binders used in this study were aqueous based colloidal silica binders, which had suspension of amorphous silica particles in water, stabilized by sodium cations. The basic chemistry of a colloidal silica binder is outlined below.

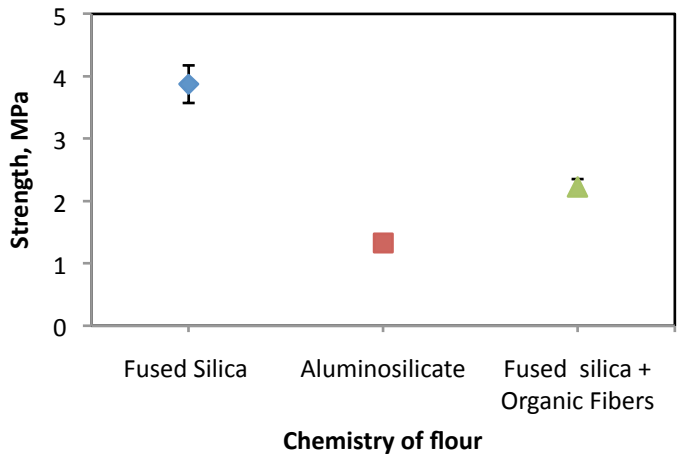

Figure 4.1: Effect of chemical composition of flour on green strength of the shell

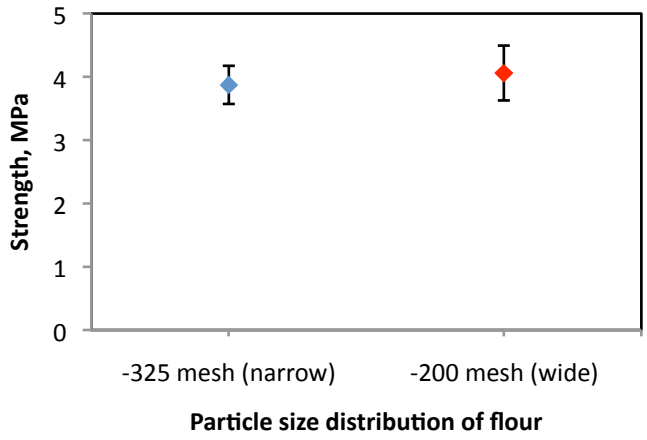

Figure 4.2: Effect of particle size distribution of flour on green strength of the shell

Amorphous silica dissolves in water forming silicic acid, $Si(OH)_4$.[25] Due to its high tendency to polymerize, siloxane bonds (-Si-O-Si-) form. A schematic of an amorphous silica particle is shown in Figure 4.3. When an alkali is added, the silanol (-Si-OH) groups on the surface get ionized and keep the particles away from each other. On drying, water is evaporated and siloxane bridges are formed between the surface silanol groups of different particles, forming a continuous network of gel. Equation 7 shows the formation of siloxane bonds.

$$\text{-Si-OH} \quad + \quad \text{HO-Si-} \quad = \quad \text{-Si-O-Si-} \quad + \quad H_2O \qquad ..(7)$$

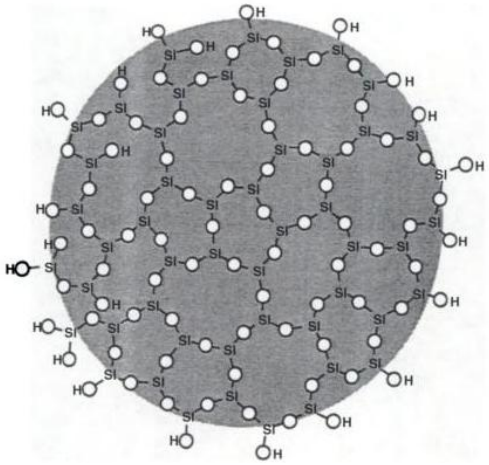

Figure 4.3: A two-dimensional schematic of a typical amorphous silica particle[25]

As the binder used for these sets of shells is the same (Megasol), the green strength should have been in the same range but significant differences were observed as shown in Figure 4.1. When aluminosilicate was used as flour, the green strength was observed to be the least with an average value of 1.33 MPa. The shells with all-fused-

silica starting materials had an average green strength of 3.87 MPa. It was observed during the shell making process that due to the high density of aluminosilicate, large amounts slurry was drained out between pattern dipping and stuccoing. This resulted in thinner shells as shown in Figure 4.4. In Figures 4.5 and 4.6, the microstructures of polished cross sections of different shells, obtained from back-scattered electron diffraction, are compared. Image analysis data for these microstructures, Table 4.1, show that the shells with aluminosilicate flour had lower amount of matrix (42.8 %) and higher porosity (20.5%) when compared to fused silica shells. Since the stucco grains were held together by a weak matrix network formed from slurry, the shells with aluminosilicate flour were found weaker.

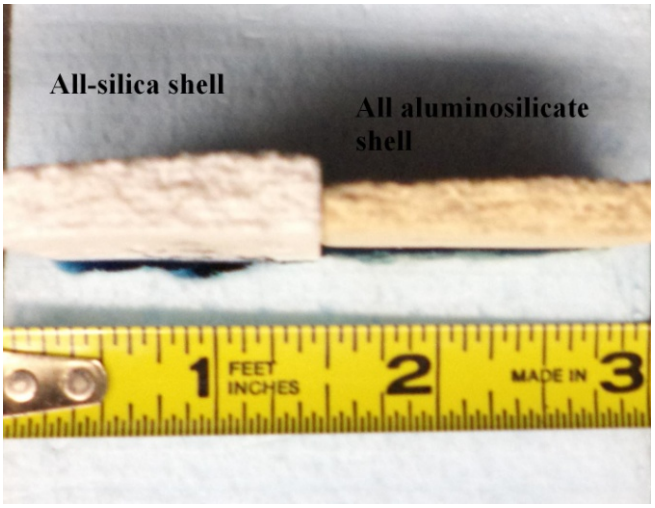

Figure 4.4: Comparison of thicknesses of shells

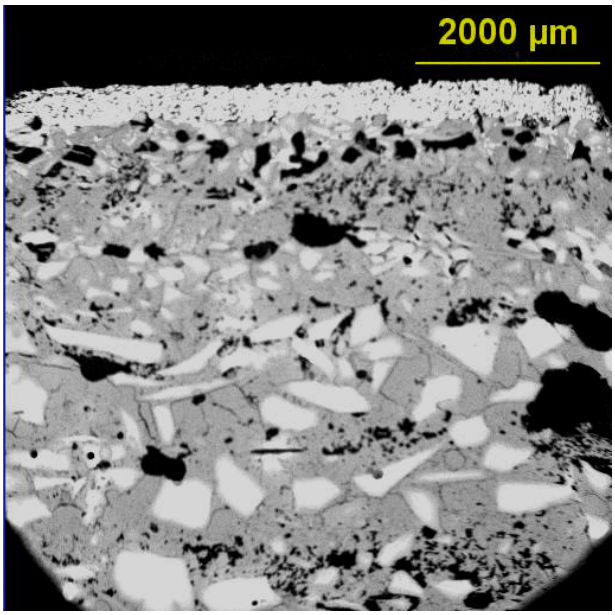

Figure 4.5: Cross-section of a shell with fused silica flour and Megasol binder

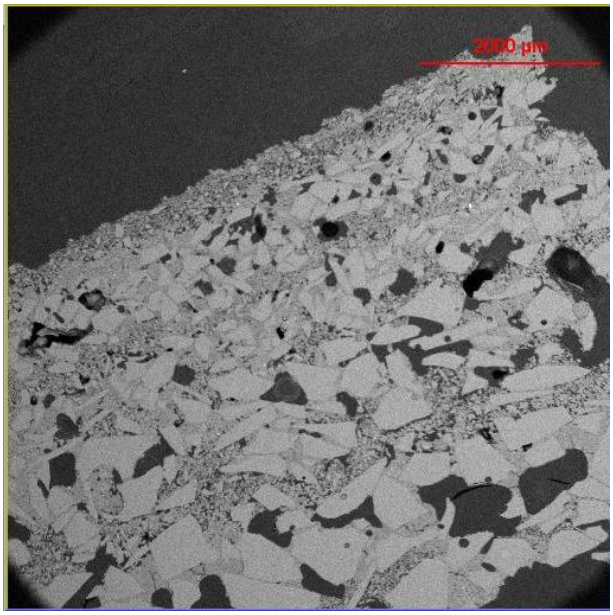

Figure 4.6: Cross-section of a shell with aluminosilicate flour and Megasol binder

Table 4.1: Image analysis data for shells with fused silica and aluminosilicate flours

	Porosity % (±5%)	Matrix % (±5%)	Stucco % (±5%)
Shells with fused silica flour	15.01	53.25	31.27
Shells with aluminosilicate flour	20.54	42.88	36.55

The use of Gray Matter, which is predominantly fused silica with polyisopropylene fibers, had also reduced the green strength of the shell (2.23 MPa). Fibers are generally added to ceramic composites to enhance the strength. In investment casting shells, fiber strengthening occurs when these fibers are aligned in such a way that they are perpendicular to the loading direction and hold the stucco grains together increasing the resistance to crack propagation. Since the fibers were introduced along the slurry, there was no control over their orientation and misalignment of fibers had resulted in a discontinuous gel network between the stucco particles. Hence the green strength was low (2.3 MPa).

4.1.1.2 Effect of stucco on green strength. The shells considered here differed only in the choice of stucco. Figure 4.7 shows that there is a small increase in the green strength when aluminosilicate stucco was used. This difference can be attributed to the microstructural changes in the gel network of these shells. It can be observed from the microstructures of these shells (Figures 4.5 and 4.8) that the fused silica grains are more angular with high aspect ratio and aluminosilicate grains are less angular. Since the green strength is controlled by the gel formed between the stucco grains on drying and as the

gel formed between the silica grains was relatively thin (Figure 4.5) the strength for these shells was observed to be less than the shells with aluminosilicate stucco.

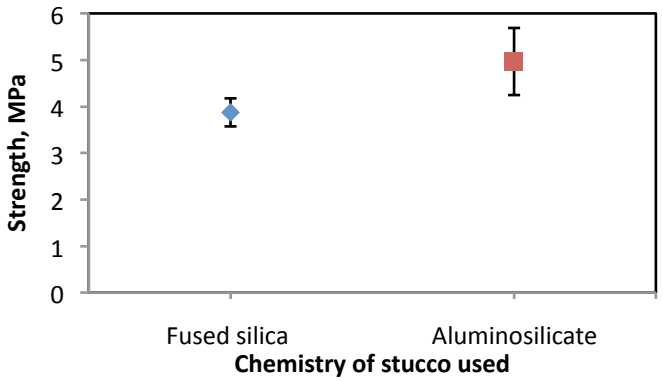

Figure 4.7: Effect of stucco chemistry on green strength of the shell

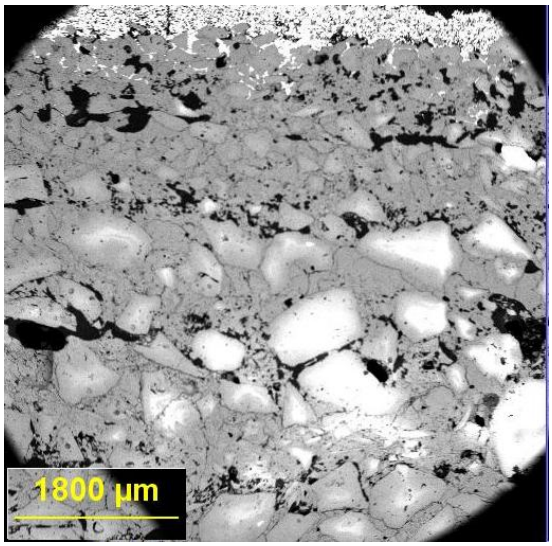

Figure 4.8: Cross-section of a shell with aluminosilicate flour and stucco

4.1.1.3 Effect of binder on green strength. As mentioned in Section 2.1.2, the work done by Boccalini et al.[6] suggests that increasing the total surface area of the binder solids increases the number of contact points between different particles increasing the

strength of the shell after sintering. But in green condition (after drying and before sintering), the gel forming behavior depends on the number of free hydroxyl groups of different particles to form siloxane bonds. The number of free hydroxyl groups depends on the alkali content of the binder. Consideration of total particle surface area along with alkali content of the binder is important when comparing green strengths. Smaller the average particle size, higher is the total surface area and more amount of alkali is required to keep the particles suspended.

To quantify this gel forming behavior of different binders, two parameters 'K_1' and 'K_2' were created, defined by equations 8 and 9. Different properties of the binders, as provided by the suppliers, were considered for these calculations. Table 4.2 compares different properties of these binders.

$$K_1 = \frac{Total\ surface\ area\ of\ the\ binder\ solids}{Total\ wt.\ of\ the\ binder\ used} \tag{8}$$

$$K_2 = \frac{Amount\ of\ alkali}{K_1} \tag{9}$$

Table 4.2: Comparison of different properties of different binders

Binder	Average particle size, nm	Silica, wt%	Na_2O, wt%	Surface area, m^2/g	K_1, m^2/g	K_2
Megasol	70 (polydispersoid)	50	0.22	70	35	6.28×10^{-3}
Nalco 1030	13 (monodispersoid)	30	0.45	230	69	6.52×10^{-3}
Nalco 1115	4 (monodispersoid)	15	0.75	750	112.5	6.66×10^{-3}

It can be observed that the ratio of the alkali available to the total surface area of the binder solids in the used amount of binder is in the same range for all the binders considered in this study. This predicts that all the shells would have the same green strength. Figure 4.9 shows that the green strengths of the shells prepared from different binders are as predicted. The addition of polymer to the binder had no effect on the green strength (Figure 4.9b). The minor variations can be attributed to the inconsistencies in process parameters.

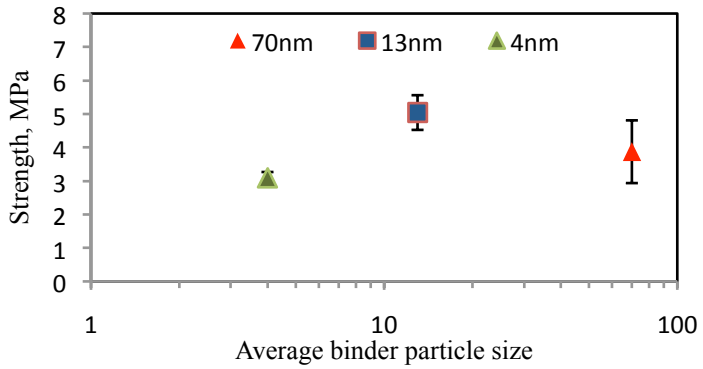

(a)

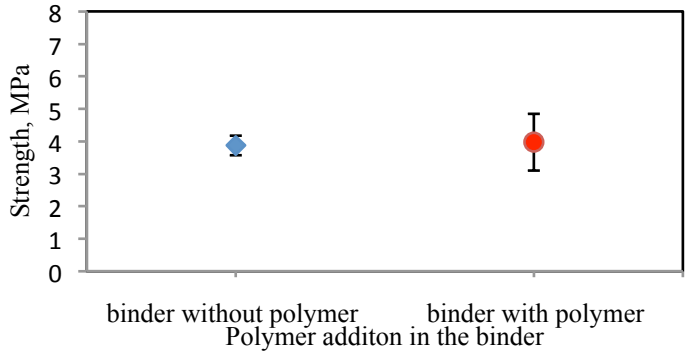

(b)

Figure 4.9: Effect of (a) binder particle size (b) polymer addition on green strength

4.1.2. Fired Strength. Flexural strength of fired test pieces was measured. The results are summarized in the following sections based on the affecting material variable(s).

4.1.2.1. Effects of chemistries of flour and stucco. The fired strengths of different shell systems are compared in Figure 4.10. To analyze the interaction behavior between stucco and matrix formed from slurry of the shell, the comparison is made between the shell systems where similar and dissimilar chemistries of flour and stucco were used. Megasol was used as binder for these shell systems.

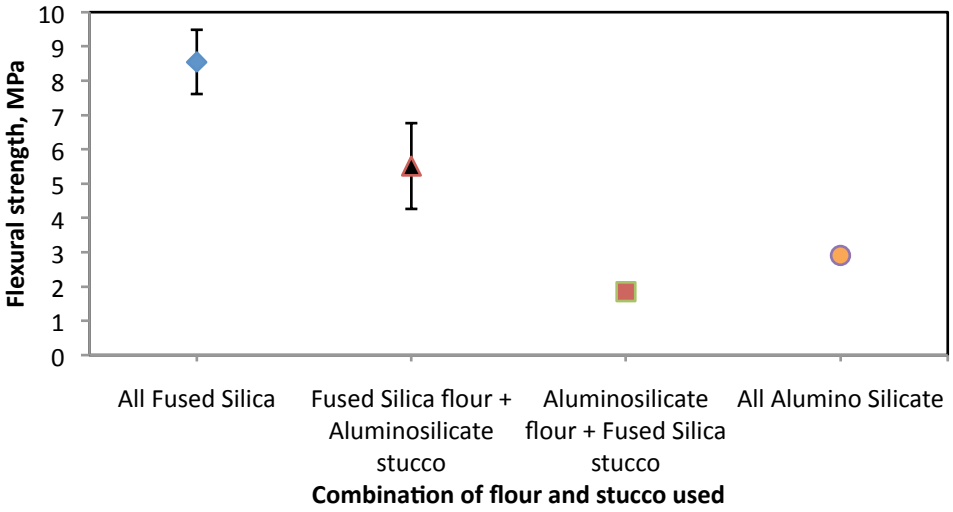

Figure 4.10: Effect of chemistry of flour and stucco on fired strength

As discussed in Section 2.3, the fracture of ceramic matrix composites depends on the relative strengths of the matrix phase and particulate phase. For all the combinations of stucco and flour used here, the fracture surfaces were observed and it was noted that the crack propagation took place through the matrix. Figure 4.11 shows a typical fracture surface of an investment casting shell. It was also observed at the time of testing that the

stucco grains were loosely bound to the matrix and were falling off. This implies that the sintering conditions used did not facilitate for the strong bonding between the matrix and stucco. The effect of the presence of porosity in the matrix is discussed in a later section.

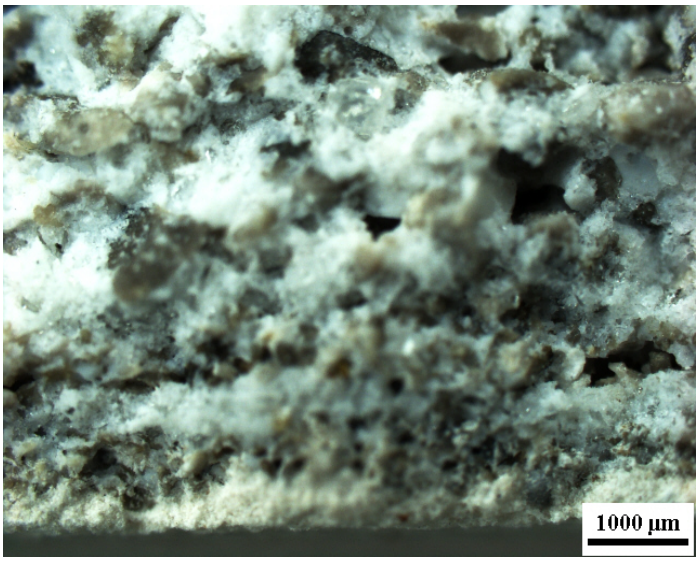

Figure 4.11: Fracture surface of a shell with aluminosilicate stucco and fused silica flour

On sintering, densification occurred resulting in enhanced strength. However, the extent of the increase in strength was different for different shells. The highest strength was observed in shells with all-fused silica-based raw materials (8 MPa) and lower strengths were observed when aluminosilicate slurry was used (2 MPa). One of the factors for lower strengths of these shells is mentioned in section 4.1.1.1, where the cross section had less amount of matrix formed from slurry. It is also important to note that when different chemistries of stucco and flour are used, during the heating and cooling cycle of sintering, there would be formation of microcracks due to mismatch in thermal expansion coefficient of fused silica (0.55×10^{-6}/°C) and aluminosilicate (5.4×10^{-6}/°C). Hence, the shells with aluminosilicate stucco on fused silica flour were weaker than all-

fused-silica shells and the shells with fused silica stucco on aluminosilicate flour were weaker than all-aluminosilicate shells.

4.1.2.2 Effects of particle size distribution of flour and particle size of binder. The effects of particle size distribution of flour and binder particle size are shown in Figures 4.12 and 4.13 respectively. There was no significant effect observed when the particle size distribution of either flour or binder was varied.

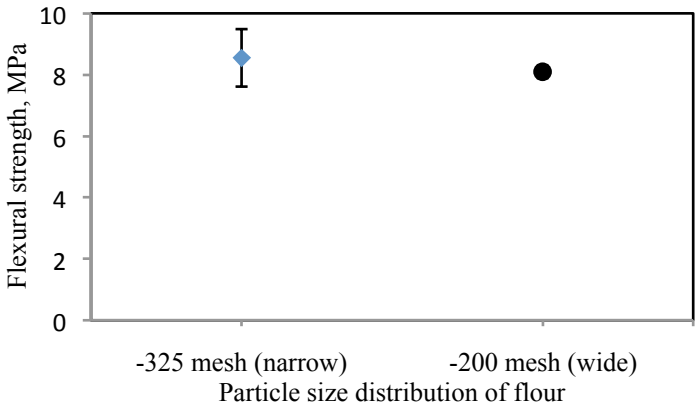

Figure 4.12: Effect of particle size distribution of flour on fired strength

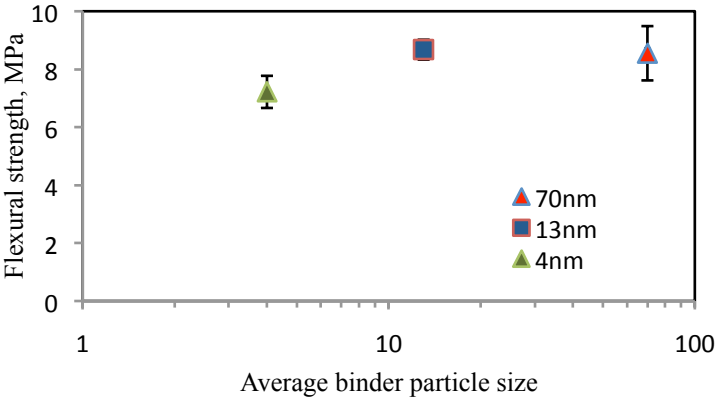

Figure 4.13: Effect of particle size of binder on fired strength

The flours compared in Figure 4.12, Ranco-Sil # 1 (-325 mesh) and Ranco-Sil # 4 (-200 mesh), had specific surface areas, 10.01 m^2/g and 7.65 m^2/g respectively (Table 3.2). The binders compared in Figure 4.13 had specific surface areas of 70 m^2/g (70nm), 230 m^2/g (13nm) and 750 m^2/g (4nm). In either case, when the surface area was increased, the fired strength was not affected significantly. Decrease in the particle size or increase in the surface area enhances the strength during sintering by increasing the number of necks formed between different particles which resist the crack propagation. Since the sintering conditions were not favorable for strengthening to take place, the fired strength was unaffected by the particle size distribution of flour and particle size of binder.

4.1.3. Hot Strength. The hot strength of the shell samples was measured using the setup shown in Figure 3.19 and effects of different material variables are discussed in the sections below.

4.1.3.1. Effect of chemistry of flour and stucco. In Figure 4.14, the flexural strengths of different shells, built from different combinations of flour and stucco, are compared. The shells with all-aluminosilicate had the highest strength and the shells with all-fused silica had the least strength.

On heating fused silica above 1000°C, devitrification of fused silica starts resulting in the formation of small amounts of β-cristobalite. Crystallization of fused silica initiates at the surface of the grains and proceeds towards the interior.[26] The kinetics of devitrification depends on various factors such as temperature, impurities in the material. This partial transformation along the surface of the grains, at 1150°C makes the crack propagation easier. Hence the fracture strength of fused silica shells was

reduced (5MPa). On cooling, β-cristobalite converts to α-cristobalite around a temperature of 250°C. This transformation is accompanied by a large volume change, which leads to formation of microcracks in the shell reducing the strength. This could help in shell removal from the casting. In Figure 4.15, the XRD plot (at 1150°C) of a fused silica shell shows the presence of cristobailte.[27]

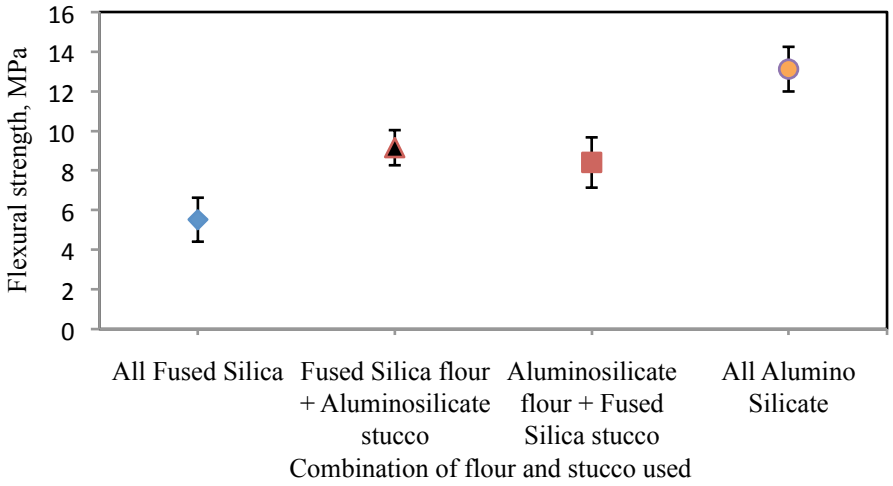

Figure 4.14: Effect of chemistry of flour and stucco on hot strength

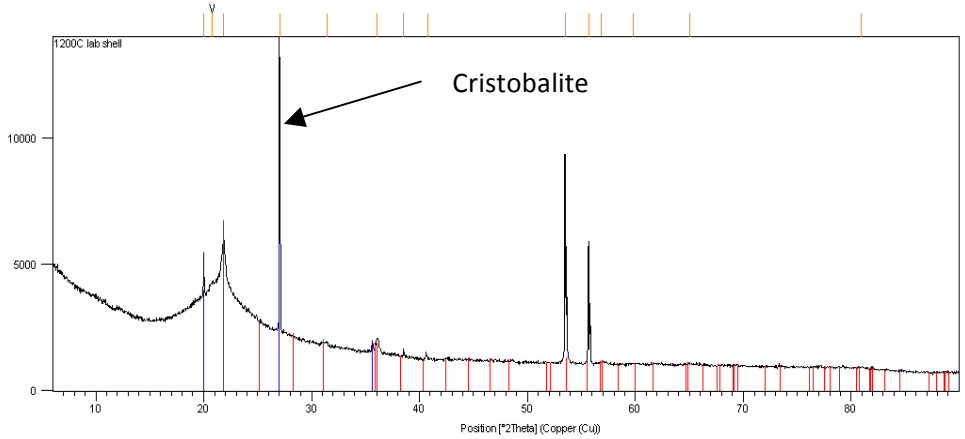

Figure 4.15. XRD pattern of fused silica shell (1150°C) showing cristobalite peaks

In shells using aluminosilicate was used as both flour and stucco, heating to 1150°C resulted in strong bonding between different particles during sintering and hence the measured strength was high (12 MPa). In the shell systems, where fused silica and aluminosilicate were used as different components of the shell, the combined effects of devitrification of fused silica and sintering of aluminosilicate have taken place resulting in strengths that are intermediate (8 - 9 MPa) of the highest and least strengths.

4.1.3.2 Effect of particle size distribution of flour and particle size of binder. The surface area effect on sintering behavior was observed only during hot strength testing. A small increase (0.8 MPa) in the average value of MOR at high temperature can be seen from the plot in Figure 4.16.

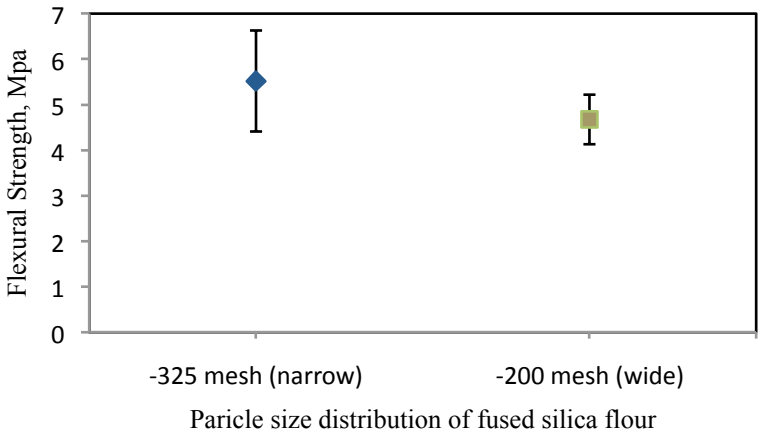

Figure 4.16: Effect of particle size distribution of flour on hot strength

While considering the effect of binder particle size on the shell strength at 1150°C, it is necessary to consider different parameters such as sintering behavior, devitrification and sodium content of the binders. As the total surface area of fused silica particles increases, sintering ability increases and also, the tendency of devitrification

increases. Devitrification rate is also enhanced by increase in sodium content.[26] From Table 4.2, it can be observed that although available cation per unit surface area of binder solids (K_2) is not significantly different for different binders, the surface area (K_1) is much higher for smaller particle binders. Hence the sintering effect was dominating and the strength was found to increase with decrease in the particle size as shown in Figure 4.17.

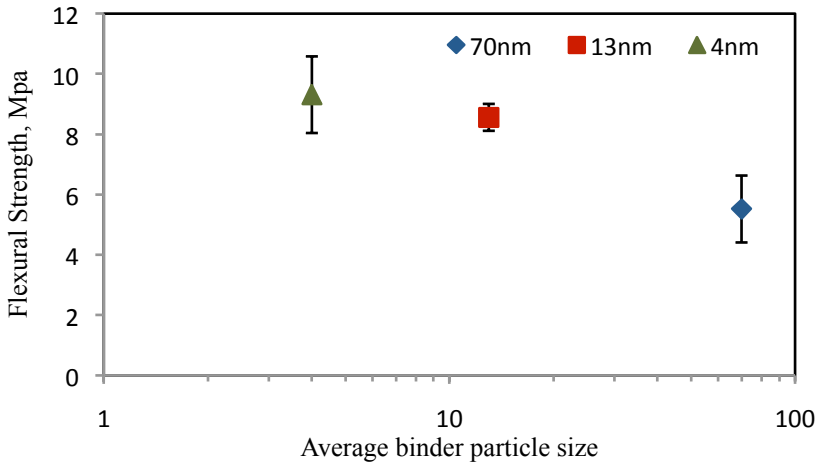

Figure 4.17: Effect of average particle size of binder on hot strength

4.1.4. Wedge Strength. Wedge shaped samples were cut and tested for strength. The wedge strength was calculated using Hyde's equation (Equation 3.3) for different shell systems and is compared with the corresponding flat bar strength (flexural strength). Figure 4.18 compares the flat and wedge strengths of shells in green and fired conditions. It was observed that the effect of different chemistries of flour and stucco on the wedge strength was similar to that on flexural strength.

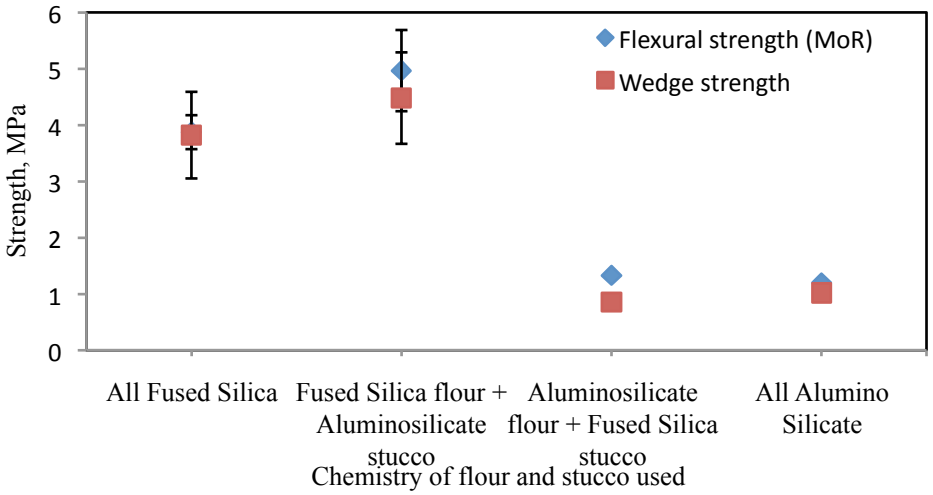

(a) Green Condition

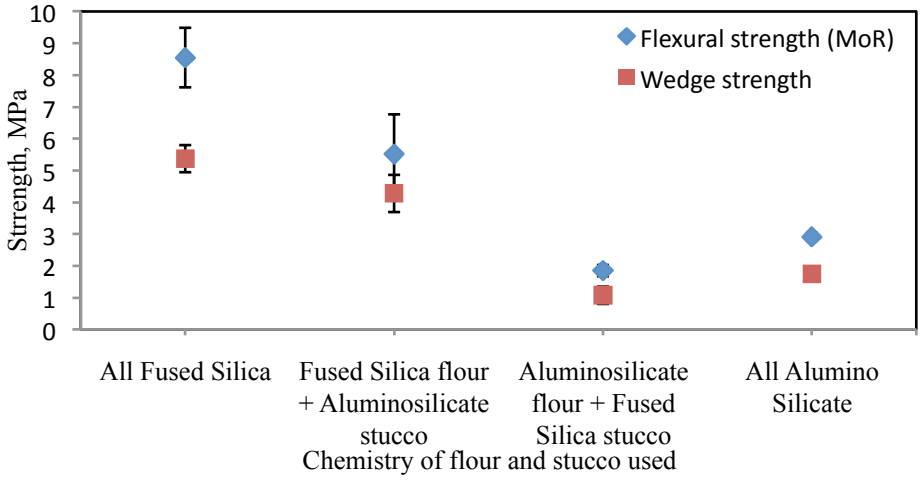

(b) Fired Condition

Figure 4.18. Comparison of wedge and flexural strengths in (a) green condition (b) fired condition for different chemistries of flour and stucco

4.2. POROSITY AND PERMEABILITY

The apparent porosity of different shell systems, determined from Archimedes principle, is shown in Figure 4.19. The measured porosity values were observed to be

varying between 20-25% for all shell systems except the shells made from aluminoslicate slurry. Higher porosity of these shells can be attributed due to the variations in the microstructure that occurred due to same reason mentioned in Section 4.1.1.1. The plots in the following figures compare the porosity of different shell systems.

The permeability of all shells considered in this study was found to be in close range (0.5 – 1 mDarcy). An earlier study[9] at Missouri S & T showed that permeability decreases with increase in viscosity of the slurry and becomes independent of the number of coatings at higher viscosities. Since the viscosity of slurry used for the prime coat for all the shells was very high (900-1000 cP), the measured permeability was very low and did not show any significant variations with any of the material variables. Figure 4.20 compares the measured permeability values plotted in 'milli-Darcy' for different shells.

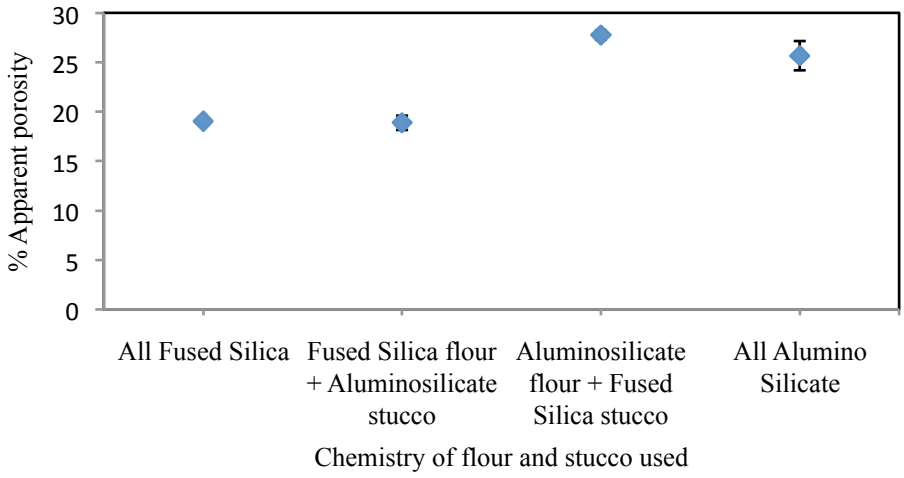

(a)

Figure 4.19: Effects of different material properties - (a) chemistry (b) binder particle size (c) flour particle size distribution and (d) fiber and polymer additives - on apparent porosity of the shell.

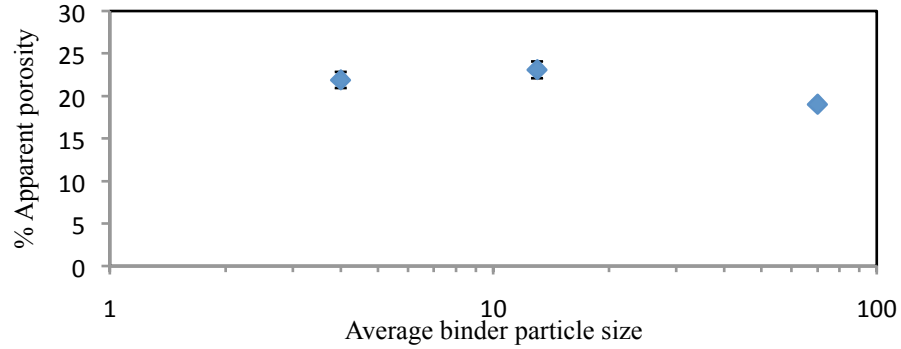

(b)

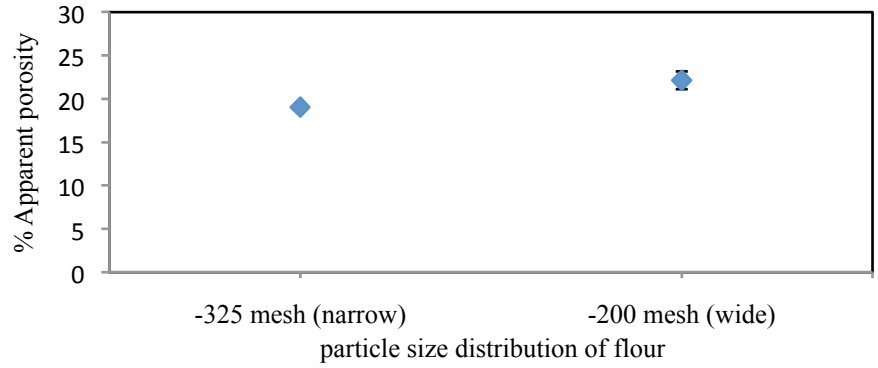

(c)

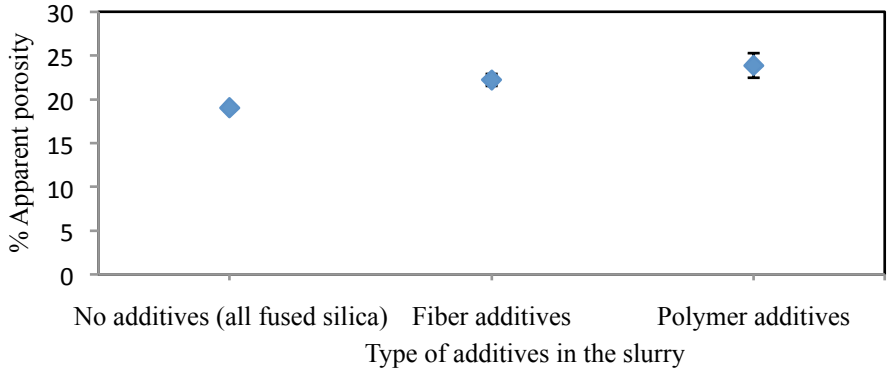

(d)

Figure 4.19: Effect of different material properties - (a) chemistry (b) binder particle size (c) flour particle size distribution and (d) fiber and polymer additives - on apparent porosity of the shell. (contd.)

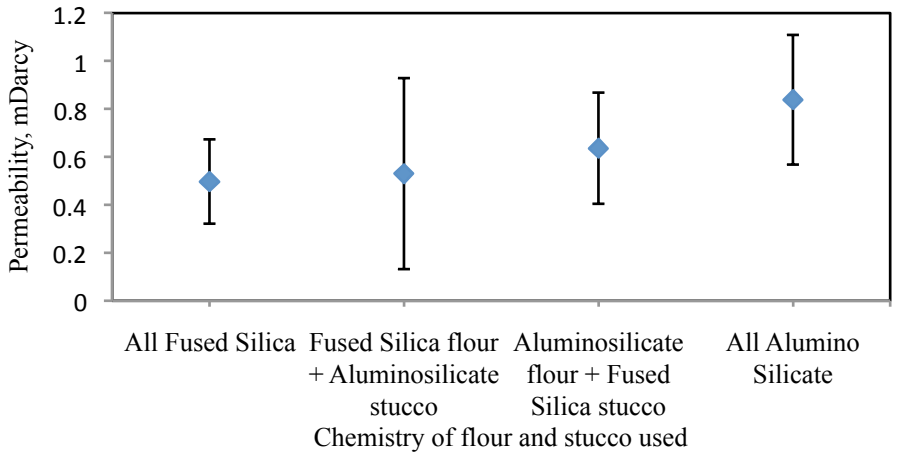

(a)

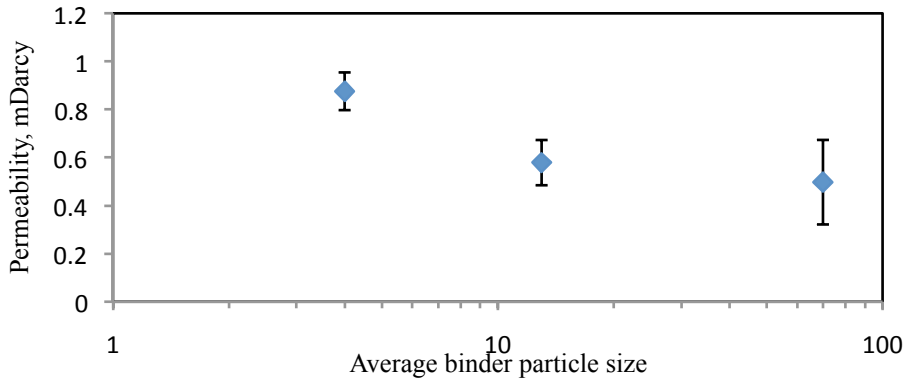

(b)

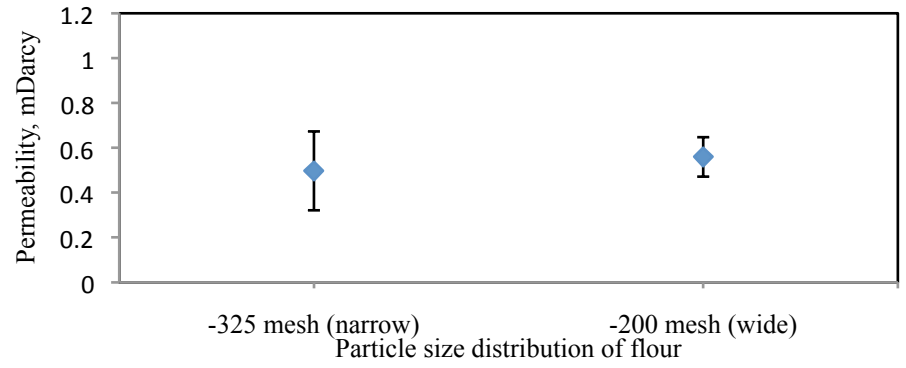

(c)

Figure 4.20: Effects of different material properties - (a) chemistry (b) binder particle size (c) flour particle size distribution and (d) fiber and polymer additives - on permeability of the shell.

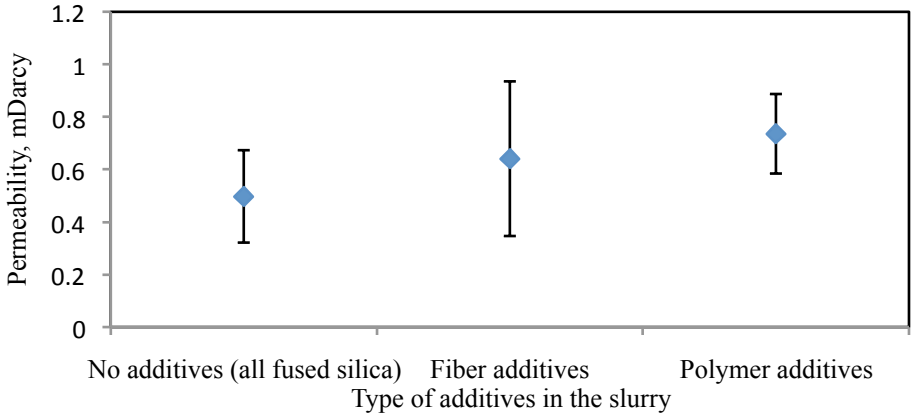

(d)

Figure 4.20: Effects of different material properties - (a) chemistry (b) binder particle size (c) flour particle size distribution and (d) fiber and polymer additives - on permeability of the shell. (contd.)

5. PROCESSING EFFECTS AND MICROSTRUCTURAL VARIATIONS IN SHELLS

To study the microstructural effects on shell properties, shells were prepared with different slurry viscosities and stucco sizes shown in Table 3.7. To ensure a homogeneous shell build among different shells within a system, a constant dipping time (30s) and a constant stuccoing time (30s) were used during the shell building process.

5.1 MICROSTRUCTURAL VARIATIONS

Polished cross sections of fired samples of shells were polished and observed for variations in the shell build. Typical microstructures of samples from each set of shells are shown in Figures 5.1 to 5.4. Different microstructural features of the cross-section (porosity, stucco and the matrix formed from the slurry) were quantified using image analysis software, ImageJ. For this quantitative analysis, the relative amounts of different constituents were determined by considering microstructures over different areas on a cross section. The data presented in Table 5.1 are the relative amounts for the total area considered.

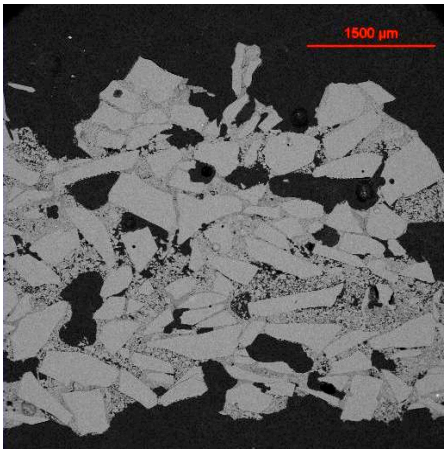

Figure 5.1: Cross-section of shell with high viscosity slurry, coarse stucco

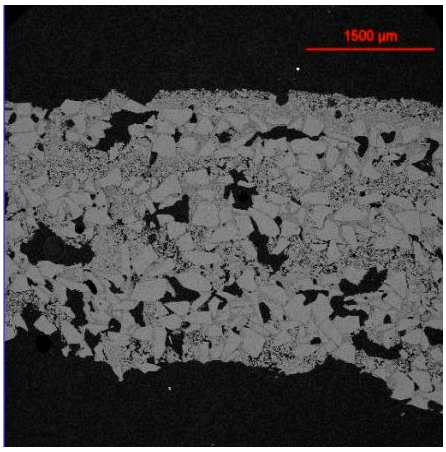

Figure 5.2: Cross-section of shell with high viscosity slurry, fine stucco

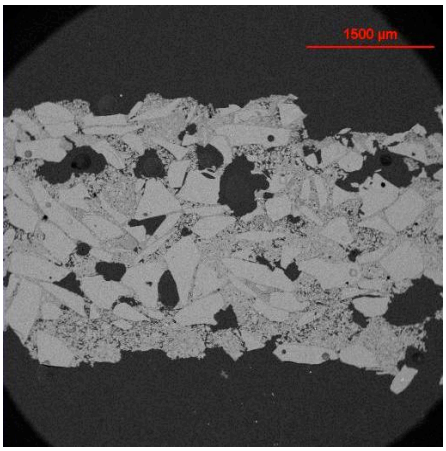

Figure 5.3: Cross-section of shell with low viscosity slurry, coarse stucco

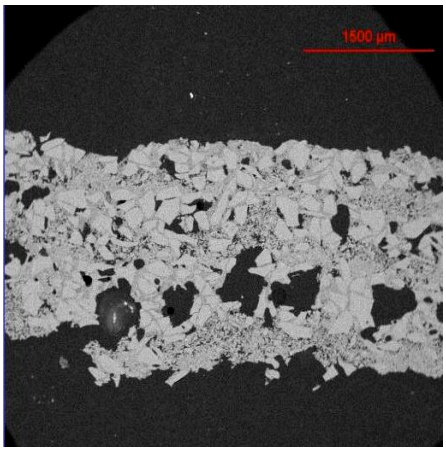

Figure 5.4: Cross-section of shell with low viscosity slurry, fine stucco

Table 5.1: Microstructural analysis and fired strengths of different shell systems

Shell System (slurry viscosity, stucco size)	Flexural strength (fired), MPa	Analysis		
		Porosity %	Stucco %	Matrix % (slurry)
i (700-800 cP, -30+50 mesh)	3.9±0.3	18.9±4.4	42.8±3.9	38.2±3.9
ii (700-800 cP, -50+100 mesh)	6.0±0.5	18.6±1.8	36.3±3.4	45.1±3.9
iii (300-400 cP, -30+50 mesh)	1.9±0.1	21.5±1.2	46.5±2.7	31.9±3.0
iv (300-400 cP, -50+100 mesh)	1.6±0.2	21.8±3.4	46.3±3.0	31.7±4.5

The shells with high viscosity slurry (700 - 800 cP) and fine stucco (-50+100 mesh) had the highest flexural strength (6.0±0.5 MPa) and the least strength (around 2 MPa) was observed for the shells with low viscosity slurry (300 - 400 cP). The results from Table 5.1 suggest that the amount of matrix across the cross-section that holds the stucco grains was a critical factor. When the amount of matrix increased, strength for a given stucco size also increased. The behaviors of these shells can be explained by considering different parameters such as total contact area between stucco and matrix, shape of stucco, sintering conditions etc. In the following section the evolution of different microstructures is discussed.

In Figure 5.5, a simple case of spherical stucco particles in a matrix formed from slurry is considered. It illustrates the differences in the distribution of stucco and matrix, when different slurry viscosities and stucco sizes are used.

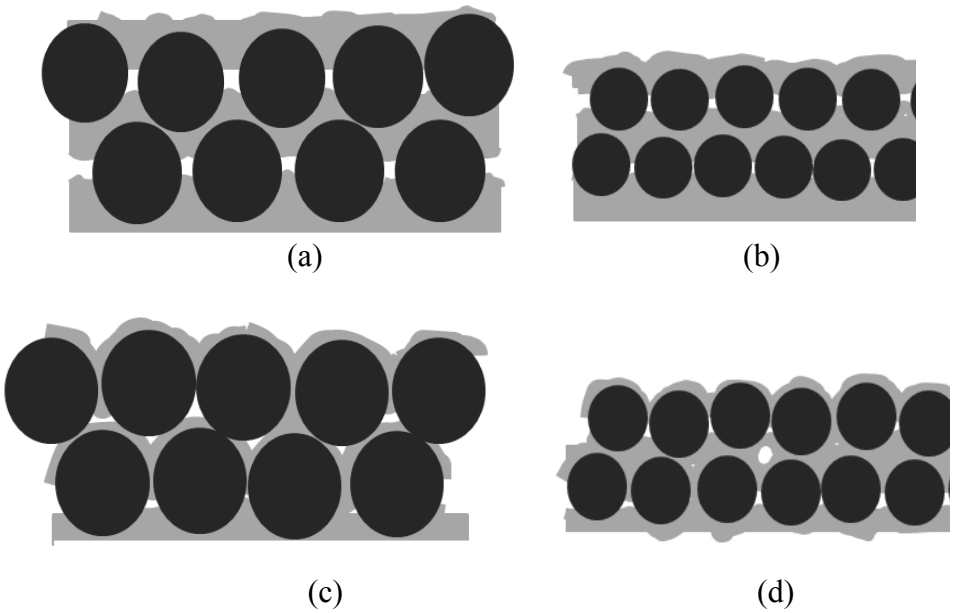

Figure 5.5: Illustration of microstructural variations when different process parameters are used (a) High slurry viscosity, coarse stucco (b) High slurry viscosity, fine stucco (c) Low slurry viscosity, coarse stucco (d) Low slurry viscosity, fine stucco

Strengths of materials with these microstructures (Figures 5.5(a) to 5.5(d)) mainly depend on:

i. Strengths of individual components
ii. Contact area between matrix and particles
iii. Porosity
iv. Sintering conditions (holding time and temperature)

Considering same material for both matrix and stucco particles, the remaining parameters are discussed here. The contact area between matrix and stucco particles depends on slurry viscosity and stucco size. For a fixed stucco size, when slurry having relatively high fluidity is used, it can penetrate easily into the gaps between stucco

particles and the contact area is increased. If the sintering conditions, such as holding temperature and time, are favorable for diffusion of material across the interface, strength would be the highest for material having large contact area. Similarly, use of fine stucco for a fixed slurry viscosity increases the contact area. These differences can be observed from Figures 5.5(a) to 5.5(d). In Figures 5.5(a) and 5.5(b), slurry could not completely penetrate and displace the air in the gaps between particles. This resulted in porosity; pore size increasing with stucco size. In Figures 5.5(c) and 5.5(d), slurry penetrated into the gaps covering all stucco particles with a thin layer. Hence the contact area and strength would be highest for the microstructure in Figure 5.5(d).

Investment casting shells compared in this study were different from the above structures in two aspects; shape of stucco and sintering conditions. Fused silica stucco particles were angular and had a range of aspect ratios. Depending on the orientation of the particles and slurry viscosity, porosity was generated. The effect of stucco shape and pore generation is illustrated in Figure 5.6. If stucco particles are aligned in such a way that the air gap between them is enclosed and slurry cannot penetrate, pores form with dimensions in the order of stucco particle dimensions.

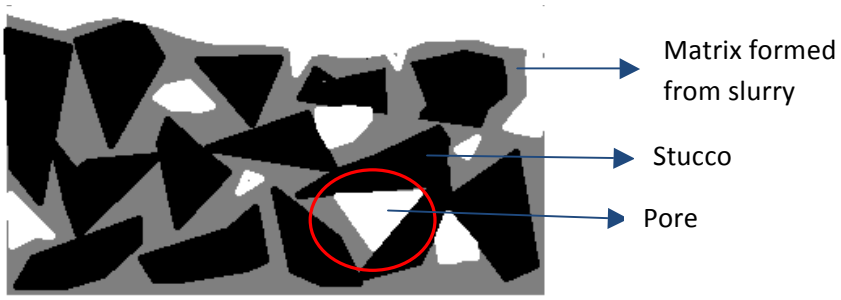

Figure 5.6. Effect of stucco shape on microstructure of shell

It was mentioned in Section 4.1.2.1 that sintering of fused silica shells, at 800°C for two hours, did not facilitate diffusion across the contact region between stucco and matrix. Hence crack propagation would be easier along the weaker regions of the cross-section; pores and matrix/stucco boundary. Based on these factors, the behavior of the shells (data from Table 5.2) can be explained. Figures 5.7(a) and 5.7(b) illustrate possible fracture paths in two different shell builds. Figure 5.7(a) is a schematic of a cross-section with finer stucco (-50+100 mesh) and higher slurry viscosity (700-800 cP) and Figure 5.7(b) is a schematic for coarse stucco (-30+50 mesh) and lower viscosity (300-400 cP). Crack propagation in a microstructure similar to Figure 5.7(b) occurs easily along the interface or pores, as indicated. When there is a relatively thicker matrix section between two stucco layers (indicated by labels A and B in Figure 5.7(a)), crack propagation occurs through breakage of siloxane bonds between different binder particles, making the overall strength higher. Hence shells with fine stucco (-50+100 mesh) and high viscosity slurry (700-800 cP) were determined to be the strongest.

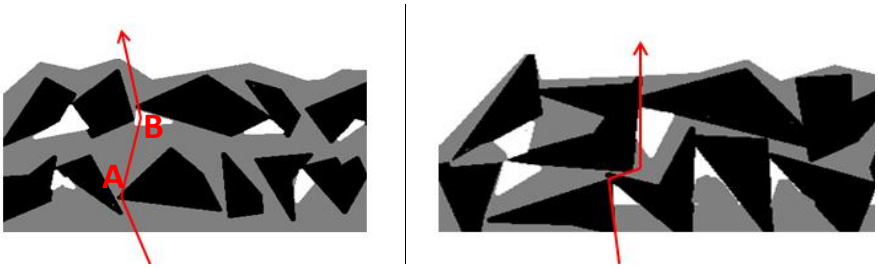

(a) (b)

Figure 5.7. Illustration of fracture path in fused silica shells (a) high viscosity slurry, fine stucco (b) low viscosity slurry, coarse stucco

The variations of flexural strength with relative amounts of matrix, porosity and stucco are plotted in Figure 5.8. The data for these plots is taken from Table 5.2.

Sample microstructures corresponding to these data points (A, B, C and D) are shown and labeled in Figure 5.9. As the porosity decreased and the amount of matrix formed from slurry increased, the strength increased. Though the decrease in porosity is not significant (2-3 %), the pore distribution and average pore size have also to be considered.

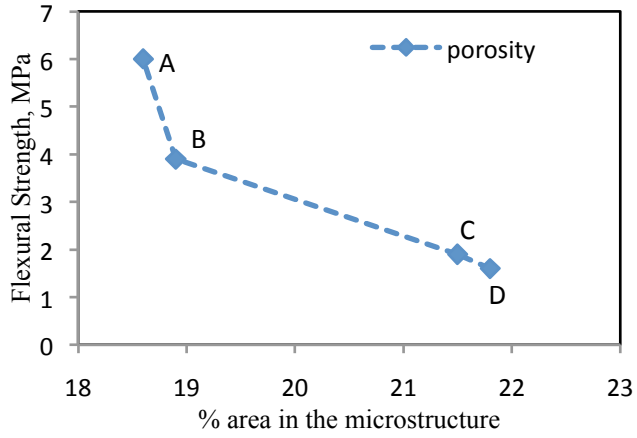

(a)

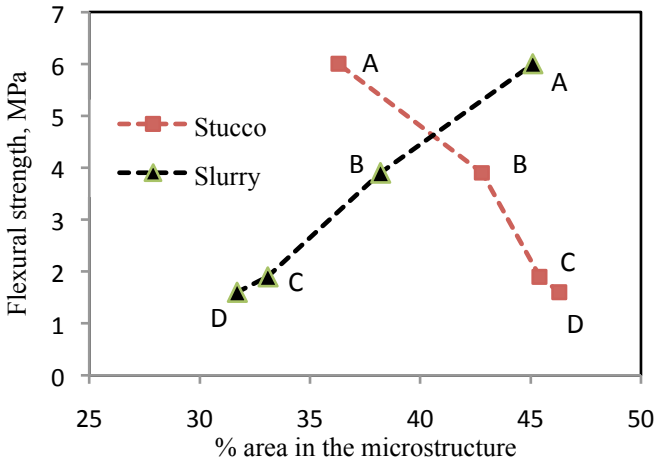

(b)

Figure 5.8. Effects of microstructural constituents; (a) % area of porosity, (b) % area of stucco and slurry matrix, on the flexural strength of a fired shell

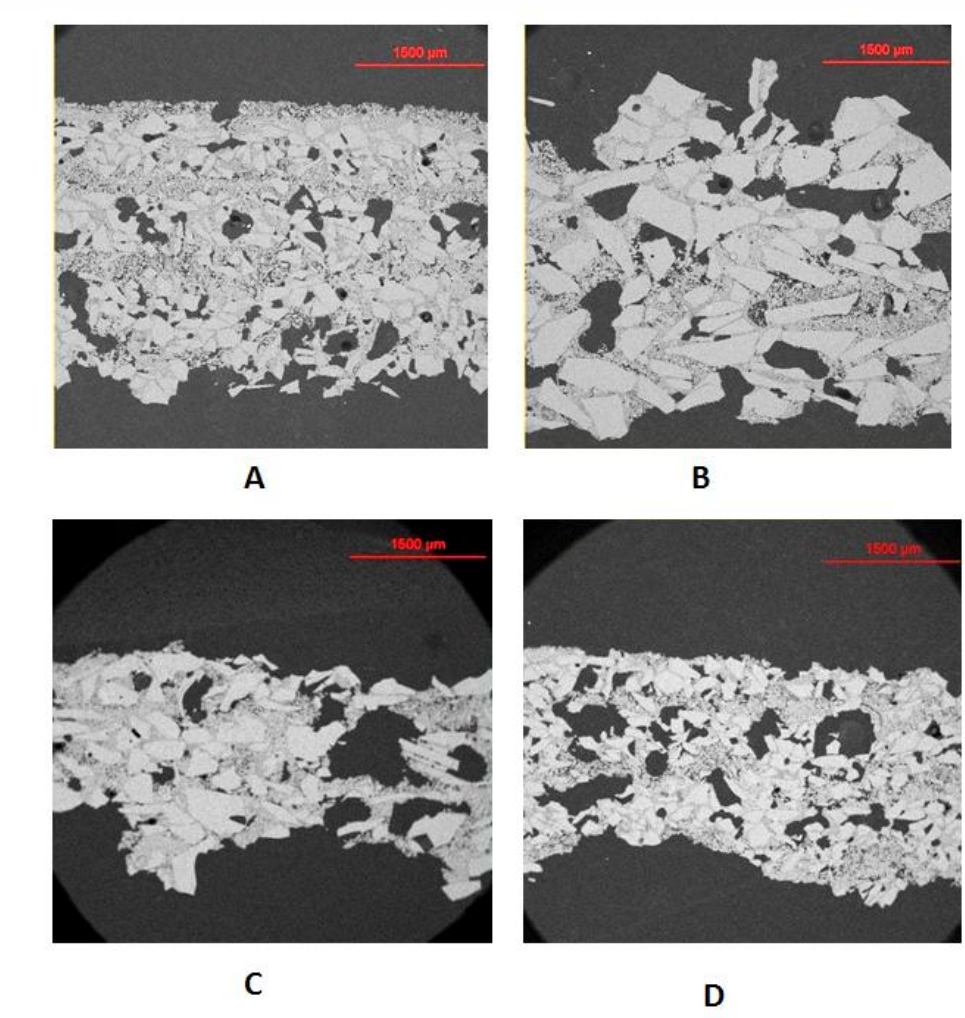

Figure 5.9. Microstructures of different shell cross-sections

5.2. VARIATIONS IN SHELL BUILD DUE TO PROCESSING PARAMETERS

The reliability of the observed effects of microstructural changes, due to slurry and stucco characteristics, in the shell depends on the process control. Homogeneous and consistent shell build is required for shells to have similar microstructure and properties. To study the variations in the material uptake during dipping the pattern in the slurry and stuccoing, the dipping time and stuccoing time were changed for different sets of shells as shown in Table 3.6.

5.2.1. Process Control. Shells were prepared in a similar way as described in the earlier sections but with a better process control. EPS foam patterns, with dimensions *3"×3"×1",* were used. Slurry viscosity used for this set of experiments was 700-800 cP. To get a uniform and similar coating thicknesses, the patterns were dipped in slurry for a constant time, allowed the slurry to drain out for a constant time by holding the pattern with the maximum dimension along the horizontal and rotating it slowly. Once the slurry stopped dripping from the pattern, slurry uptake was measured. Stucco was then applied using rainfall sander, while the pattern was being held and rotated along the axis through maximum dimension. The stucco uptake was then measured. The data points plotted were the average values of three readings. The standard deviation for all of the following readings was 5% - 10%.

5.2.2 Results and Discussions. Figures 5.10 and 5.11 show the variation of slurry uptake with the dipping time, for different coatings. The stuccoing time was 20s for these shells. Figure 5.10 compares the shells with coarse stucco (-30+50 mesh) and Figure 5.11 compares the shells with fine stucco (-50+100 mesh) was used. It was observed that when coarse stucco was used, slurry uptake increased from primary coat towards the backup coats. No specific trend was followed in case of shells with fine stucco.

It can also be observed from Figure 5.10 that slurry uptake increased with dipping time, approaching a maximum at 20s. Similar trend was observed in shells with fine stucco (Figure 5.11)

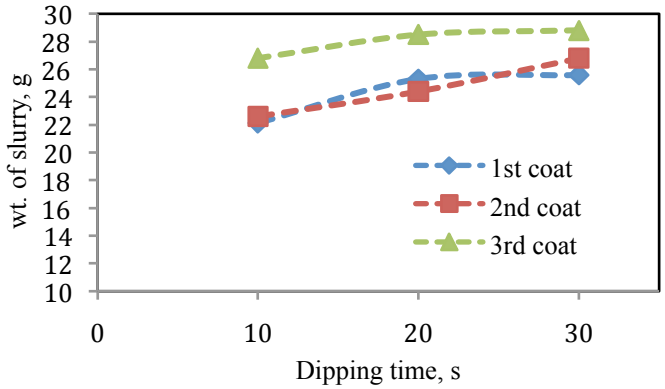

Figure 5.10. Variation of slurry uptake when coarse stucco is used

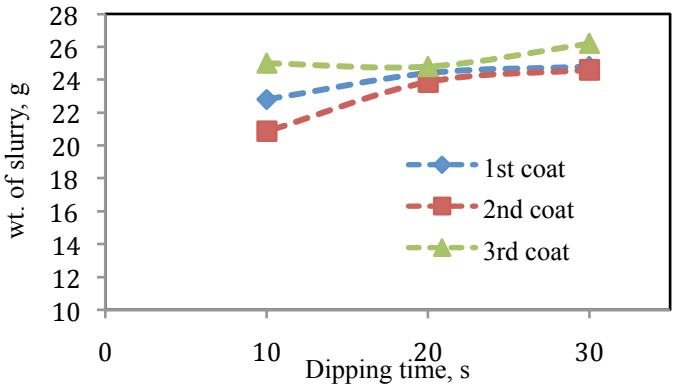

Figure 5.11. Variation of slurry uptake when fine stucco is used

Porosity generation, when coarse (-30+50 mesh) fused silica is used, is explained in section 5.1. In multilayer coatings, pores generated during subsequent coatings can be interconnected giving rise to a channel through which slurry can penetrate during dipping. A simple illustration of this is shown in Figure 5.12(a). The extent of slurry flow through interconnected porosity depends on slurry viscosity and dipping time. Effect of viscosity was not considered here. Slurry uptake up to three coatings was measured. As the number of back-up coats increases, the length of channel formed from pores may increase resulting in a higher uptake. Higher increase (~4 g) in slurry uptake in the third

coat is an indication of this (Figure 5.10). When a shell is dipped in slurry, due to fluid pressure, it penetrates into the shell displacing the air in the pores. Dipping time affects the amount of slurry added. Figure 5.10 shows that slurry uptake approached a maximum after 20s for third coating. This time can be higher for further back-up coats. Use of fine stucco (-50+100 mesh) results in a cross-section similar to Figure 5.12(b), with fine pores between different. Hence increase in slurry uptake for back-up coats was observed to be insignificant.

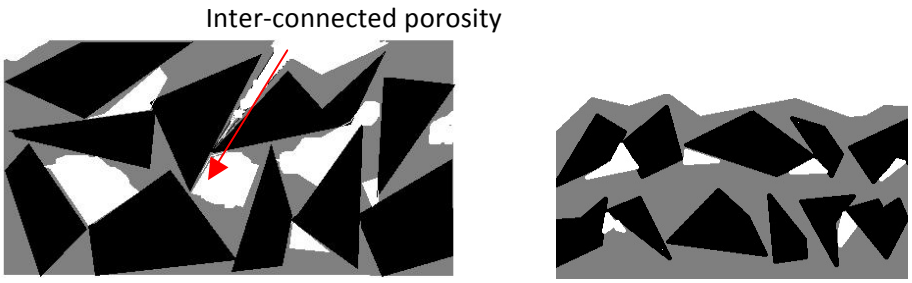

(a) (b)

Figure 5.12. Porosity in shells with different stucco sizes (a) -30+50 mesh (b) -50+100 mesh

Similarly, the variation of stucco uptake at a constant dipping time is shown in Figures 5.9 and 5.10, which correspond to coarse (-30+50 mesh) and fine stucco (-50+100 mesh) respectively. In both cases, the amount of stucco attached is the least on the prime coat. The first coating of slurry would have smooth surface and for a given slurry viscosity, stucco uptake depends on the available surface area. While making back-up coats, after dipping shells in slurry, the surface becomes rough due to the presence of stucco (Figure 5.12). In addition, the overall dimensions of the pattern increase, making the available surface area higher that can accommodate more stucco particles on the pattern. Hence the stucco uptake increased for backup coats in both cases. Once the

pattern or the shell is completely covered with a stucco layer, extra particles would strike and fall off the pattern. There would be a time after which a pattern cannot take anymore stucco. In this case, maximum uptake for both coarse and fine stucco was observed at 20s. Different factors should be considered while measuring the material uptake during dipping and stuccoing such as precision in slurry viscosity measurement, orientation of the pattern while dipping and stuccoing to make sure total surface of the patterns are equally affected during slurry draining or stuccoing etc. The large variations (5% -10%) in these data were possibly due to due to human errors or equipment inconsistencies.

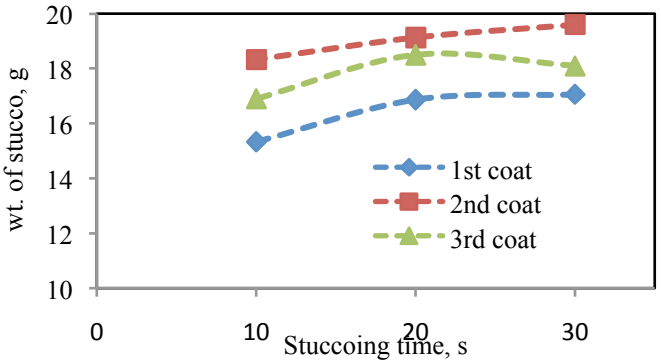

Figure 5.13. Variation of stucco uptake when coarse stucco is used

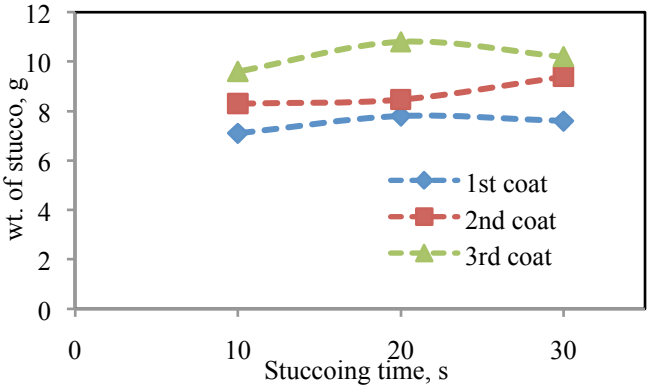

Figure 5.14. Variation of stucco uptake when fine stucco is used

6. CONCLUSIONS AND RECOMMENDATIONS

6.1. CONCLUSIONS

The effects of material and process parameters on the mechanical behavior of investment casting shells had been analyzed in this research. The flexural strength was observed to be affected by different variables in different testing conditions.

The results of shell systems listed in Table 3.6 show that green MOR was dominantly affected by the gel forming behavior of the binder and also the type of shell build (relative amounts of stucco and matrix) across the cross-section. It varied from 3.8 MPa for the shells with fused silica flour to 1.3 MPa for the shells with aluminosilicate flour (Figure 4.1). Fired and hot strengths were observed to vary with the interactions between different phases in stucco and matrix, results summarized in Figure 6.1. Strengthening due to sintering (13.1 MPa) was evident in all-aluminosilicate shells at high temperature (1150°C). Devitrification of fused silica resulted in the reduction of shell strength (from 8.55 MPa to 5.52 Mpa) at 1150°C.

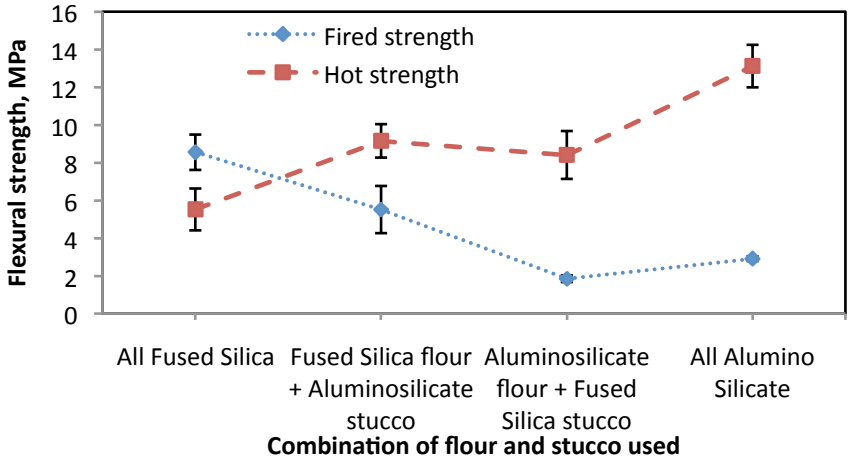

Figure 6.1: Effects of different material chemistries on fired and hot strengths.

Evolution of different microstructures, when slurry viscosity and stucco size were varied, was studied. The highest shell strength (6.0 MPa) was observed when high viscosity slurry (700-800 cP) and fine stucco (-50+100 mesh) was used. Shells built from low viscosity slurry (300-400 cP) were weaker irrespective of the stucco size. Image analysis of different microstructures showed that the shells were stronger when the cross-section contains higher amount of matrix formed from slurry (45% - 50%) and lower porosity (18% - 20%).

The microscopic observations of the shells by scanning electron microscope, as described in Section 5.1, can be used as a tool to study the critical features of the shell build. This quantitative and qualitative image analysis helps for a better understanding of the fracture of the shell.

6.2. RECOMMENDED SHELL BUILDING PROCESS

Based on the observations from this research, a detailed process to build a shell with is described here. The starting materials considered here are all fused silica products since these shells were observed to have the highest green (4-5 MPa) and fired (7-8 MPa) strengths. Ranco-Sil # 1 is considered as flour, Ranco-Sil as stucco and Nalco 1115 as binder. Patterns considered are EPS foam patterns with the dimensions *3″×3″×1″*.

6.2.1. Slurry Preparation. The recommended parameters for slurry making are outlined below.

i. Slurry preparation can be done at room temperature. Filling ratio (flour weight/binder weight) for primary coat is 2.5:1 and for back-up coats is 2:1. Slurries for primary coats and back-up coats should be prepared separately. Take the binder in a

container and add the flour slowly into it while the both are being mixed simultaneously with a high shear mixing equipment (>1000 RPM).

ii. Keep mixing binder and flour till a homogeneous mixture without any lumps is formed. Then place the container in a setup where there is low shear mixing (rotating tank with less than 100 RPM) and allow the slurry to stabilize for at least 24 hours. Usually rotating tanks are used for this. Propeller mixing is not recommended since it creates a vortex in the system, which would introduce air bubbles into the slurry.

iii. Adjust the viscosity of the slurry by adding distilled water. For the primary coat slurry, a viscosity of 800-900 cP is required and for back-up coat slurries, 400-500 cP is required. If the measured viscosity is lower than required, set the dehumidifier in the room to a lower value (relative humidity of 30%) so that viscosity increases quickly.

6.2.2. Pattern Making. Foam patterns need to be polished uniformly with 180-grit sand paper to improve adhesion of slurry to the surface of the pattern. For efficient handling of the pattern during shell building, extensions (made of relatively harder material), with dimensions *1"×1"×0.5"*, are glued to the patterns along the axis through the maximum dimension.

6.2.3. Shell Making. Fine stucco (-50+100 mesh) is used for primary coat and first back-up coat. Coarse stucco (-30+50 mesh) is used for rest of the back-up coats. Different steps of shell making are listed below.

i. For both primary and back-up coats, dip the pattern into the slurry slowly, hold it for 20s and then remove it. Allow the slurry to drain off by holding the pattern with the maximum dimension parallel to horizontal and keep it rotating slowly for 90s.

ii. While stuccoing, hold the pattern inside the rainfall sander and keep it rotating along different axes. Total time of stuccoing is 20s for all coats.

iii. After stuccoing allow the shells to dry before the next coating for four hours in the presence of a dehumidifying atmosphere (relative humidity: 40% or less).

iv. Repeat these procedures till a total of six coatings are applied. Allow the completely built shells for a day before pattern removal.

6.2.3. Pattern Removal and Firing. Dissolve the foam in the molds using acetone. Pour acetone into the mold cavities and once the foam is dissolved, drain out the remaining liquid. Allow the molds to dry for an hour before firing.

Keep the shells in a furnace and heat them to a temperature of 850°C, with a heating rate of 5°C/min. Hold the furnace at 850°C for two hours and switch it off. Leave the shells in the furnace with the door closed and let them cool back to room temperature.

6.2.4. Pre-heating the Mold and Casting. Before pouring the liquid metal into the molds, heat them to a temperature of 900°C (heating rate 5°C/min) in a furnace. Once the liquid metal is ready, place the pre-heated molds in the pouring floor and pour the metal into the mold. The shell is removed from the casting when the liquid metal is solidified.

6.3. RECOMMENDATIONS FOR FUTURE WORK

The primary focus of this research was on the mechanical behavior of shells during investment casting process. Some of the other important properties required for the investment casting shells were not explored in this study. Following are some recommendations for further study that could help in enhancing different shell properties.

6.3.1. Effects of Microstructure Variations on Permeability. Sufficient permeability of the shell is required for a sound casting and better pattern burnout. Changing the microstructure of the shell changes the pore network that affects the rate of gas flux through the shell. The microstructural effects, arising due to different material and process parameters, on permeability can be studied by changing the shell build.

6.3.2. Thermal Conductivity Dependence on Microstructure. Thermal conductivity of the shells also changes with the relative amounts of porosity, stucco and matrix formed from the slurry. It is sensitive to the chemistry of refractories used in the primary coats. A modified laser flash test can be used to study the effects on thermal conductivity.[28]

BIBLIOGRAPHY

1. P.R. Beeley, R.F. Smart, “Investment Casting”, The Institute of Materials, 1995.

2. Investment Casting Handbook, ICI, 1980.

3. ASM Handbook, Vol 15, ASM International, 2008.

4. David Viers et al., Improved Shell Knockout Properties, Investment casting Institute, 51st technical conference and expo, 2003, 12.1-12.8.

5. Marti Rothlisberger, Slurry Building Techniques and Slurry Control Processes – Keys to high quality ceramic shells.

6. M. Boccalini Jr. and E. Correa, Effect of binder/filler ratio on hot strength and hot permeability of investment casting ceramic moulds, International Journal of Cast Metals Research, vol 9, 1996, 133-137.

7. R.L. Rusher, Strength Factors of Ceramic Shell Molds, AFS Cast Metals Research Journal, 1974, 10, 149-153.

8. Charles H. Maztek, The Effect of Slurry Viscosity and Stucco Size on Shell Properties, REMET Corporation.

9. D.M. Kline, Thesis, Missouri S & T, 2010.

10. Charles H. Maztek, Using stucco more efficiently, REMET Corporation.

11. S. Jones, C. Yuan, M. R. Jolly, Fluid Bed and Rain Fall Sanded Shells – An Investigation Into Fundamental Structural and Mechanical Property Differences, Investment casting Institute, 51st technical conference and expo, 2003, 14.1-14.29.

12. Manuel Guerra Jr., REMET Laboratory, Factors Affecting Shell Strength and the Effect of Dry Time on Shell Strength, 22nd EICF Conference, April 1992.

13. Michael J. Hendricks et al., The effect of seal dips on ceramic shells properties and performance, Investment Casting Institute, 50th technical conference and expo, 2002.

14. Michael J. Hendricks, Daniel W D Hsu, Processing and Firing influences on ceramic shell materials, Foundry Trade Journal, 1991.

15. F.M. Wahl, R.E. Grim and R.B. Graf, Phase transformations in Silica as examined by continuous x-ray diffraction, The American Mineralogist, Vol.56, 196-208, 1961.

16. N.G. Ainsle et al., Melting kinetics of quartz and cristobalite, Journal of Physical Chemistry, vol.65, No.10, 1718-1724, 1961.

17. R.C. Feagin, REMET Corporation, Characteristics of Some Alumino-Silicates Colloidal Silica Shell Systems, 26th annual meeting of ICI, 1978.

18. Snow J D, Scott D H, Comparing Fused Silica and Alumino-silicate Investment Refractories, Modern Casting, Jan 2001, Vol 91, No. 1, P 45-47.

19. Michael J. Hendricks et al., Hot MOR, Creep Properties of Common Ceramic Shell Refractories, Modern Casting, Vol 89, Issue 1, Pg.44, Jan 1999.

20. C. Yuan and S. Jones, Investigation of fiber modified ceramic molds for investment casting, Journal of the European Ceramic Society, vol.23, 2003, 399-407.

21. S. Jones, C. Yuan, and K. Lewis, Organic fiber modified ceramic shell molding for investment casting, Institute of Materials, Minerals and Mining, 2002.

22. Roy W. Rice, Porosity of Ceramics, 1998.

23. R.L. Coble and W.D. Kingery, Effect of porosity on physical properties of sintered alumina, Journal of the American Ceramic Society, Vol.39, No.11, 377-385.

24. L. Coronel, J.P.Jernot and F.Osterstock, Microstructure and mechanical properties of sintered glass, Journal of Materials Science, Vol.25, 4866-4872, 1990.

25. I.M.Low, Ceramic Matrix Composites – Microstructure, Properties and Applications, 2006.

26. Horacio E. Bergna, Colloid Chemistry of Silica, Advances in Chemistry; American Chemical Society, 1994.

27. Chirag Mahimkar, Thesis, Missouri S & T, 2011.

28. Mingzhi Xu et al., Measurements and Confirmation of Thermal Properties of Investment Ceramic Shell by Multiple Methods, AFS Transactions, Vol.120, No.12-023, 229-236, 2012.

VITA

Priyatham Tumurugoti was born in Nalgonda, India. In April 2002, he graduated from Siddhartha High School after completing his SSC. In May 2004, he graduated from New Generation Junior College after completing Intermediate education. He graduated from Indian Institute of Technology Madras, Chennai, India in July 2009 with a B.Tech degree in Metallurgy and Materials Engineering. From August 2009 to July 2010, he was employed as Management Trainee in Steel Authority of India Limited, India. In May 2013, he received his M.S. Degree in Materials Science and Engineering from Missouri University of Science and Technology, Rolla, MO, USA.

During the Masters, he has published and presented an article "Strength of Investment Casting Shells – Material and Microstructure Effects" in Investment Casting 59th Annual Technical Meeting and Expo, Nashville, Tennessee.